J. Electrochem. Sci. Eng. **13(4)** (2023) 687-711; http://dx.doi.org/10.5599/jese.1704

Open Access : : ISSN 1847-9286
www.jESE-online.org

Original scientific paper

Cathode reaction models for Braga-Goodenough Na-ferrocene and Li-MnO_2 rechargeable batteries

Masanori Sakai✉

Tenjinbayashicho 1225-144, Hitachiota-shi, Ibaraki 3130049, Japan

Corresponding author: ✉*sakaimasanori144@gmail.com; Tel: +81-80-7179-3084; Fax: +81-294-73-1880*

Received: February 13, 2023; Accepted: May 4, 2023; Published: May 24, 2023

Abstract

Braga-Goodenough all-solid-state Na-Fc and Li-MnO_2 batteries demonstrate deposition of Na and Li on the cathode during discharge. These reaction mechanisms were investigated in light of the generalized charge neutrality level and the experimental results of Braga et al.*, and two new types of mechanisms were proposed. The Na-Fc mechanism is represented by a multi-step C[(CE)cC]n mechanism where C is the chemical step, E is the electrochemical step, c is the catalytic (CE) step, and n denotes the number of [(CE)cC] part cycles. The n^{th} cycle corresponds to* n *moles of Na and Li deposition. For Li-MnO_2, two mechanisms were considered. One is the C[(CE)cC]n mechanism which is the same as Na-Fc, and the other is the C[2(CE)cC]n mechanism, which involves two consecutive (CE)c steps. In the C step of (CE)c of both mechanisms, Fc and MnO_2 reduce $Na^+_{(sf)}$ and $Li^+_{(sf)}$ (sf - surface states) to deposit Na and Li, respectively, which are intramolecular charge transfer reactions within the adsorbed molecules. Fc and MnO_2 are oxidized to intermediates immediately reduced to Fc and MnO_2 by their anodes in the subsequent E step. Based on these mechanisms, these batteries' discharge capacity and cathode alkali metal deposition were examined in detail.*

Keywords

Alkali metal battery; all-solid-state battery; Li deposition; Na deposition; ferrocene; manganese dioxide

List of symbols

Fc	ferrocene, $Fe(C_5H_5)_2$
Na-Fc	sodium-ferrocene all-solid-state rechargeable battery
Li-MnO_2	lithium-manganese dioxide all-solid-state rechargeable battery
Li-S	lithium-sulfur all-solid-state rechargeable battery
ϕ^G_{CNL}	generalized charge neutrality level
ϕ_{CNL}	charge neutrality level
Na^+gl^-	Na-glass solid electrolyte of $Na_{2.99}Ba_{0.005}O_{1+x}Cl_{1-2x}$
Li^+gl^-	Li-glass solid electrolyte of $Li_{2.99}Ba_{0.005}O_{1+x}Cl_{1-2x}$
(sf)	surface states

$Na^+_{(sf)}$	Na^+ in surface states of $Na_{2.99}Ba_{0.005}O_{1+x}Cl_{1-2x}$
$Li^+_{(sf)}$	Li^+ in surface states of $Li_{2.99}Ba_{0.005}O_{1+x}Cl_{1-2x}$
C	chemical reaction
E	electrochemical reaction
c in C[(CE)cC]*n*	catalytic reaction steps
c in C[2(CE)cC]*n*	catalytic reaction steps
n in C[(CE)cC]*n*	number of cycles of the [(CE)cC] part
n in C[2(CE)cC]*n*	number of cycles of the [2(CE)cC] part
2 in C[2(CE)cC]*n*	two consecutive (CE)c
HOMO	highest occupied molecular orbital
LUMO	lowest unoccupied molecular orbital
$FcNa^+_{(sf)}$ (ad)	adsorbed molecule between Fc and $Na^+_{(sf)}$
$MnO_2Li^+_{(sf)}$ (ad)	adsorbed molecule between MnO_2 and $Li^+_{(sf)}$ for C[(CE)cC]*n*
$MnO_2[2Li^+_{(sf)}$ (ad)]	adsorbed molecule between MnO_2 and $2Li^+_{(sf)}$ for C[2(CE)cC]*n*
high-*k*	high relative permittivity
$\lvert t_{VB\text{-}CB'}\rvert$	transfer energy between the valence band orbital of Fc and the conduction band orbital of $Na^+_{(sf)}$ or transfer energy between valence band orbital of MnO_2 and conduction band orbital of $Li^+_{(sf)}$
$\lvert t_{VB'\text{-}CB}\rvert$	transfer energy between the valence band orbital of Na^+gl^- and the conduction band orbital of Fc or transfer energy between the valence band orbital of Li^+gl^- and the conduction band orbital of MnO_2
E_f	Fermi level
E_{CB}	energy level of the conduction band bottom for Fc or MnO_2
E_{VB}	energy level of the valence band top for Fc or MnO_2
E'_{CB}	energy level of the conduction band bottom for Na^+gl^- or Li^+gl^-
E'_{VB}	energy level of the valence band top for Na^+gl^- or Li^+gl^-
E'_g	band gap, E'_{CB} - E'_{VB}, for Na^+gl^- or Li^+gl^-
D_{VB}	density of states of the valence band for Fc or MnO_2
D_{CB}	density of states of the conduction band for Fc or MnO_2
D'_{VB}	density of states of the valence band for Na^+gl^- or Li^+gl^-
D'_{CB}	density of states of the conduction band for Na^+gl^- or Li^+gl^-
Ψ	$(\lvert t_{VB\text{-}CB'}\rvert^2/\lvert t_{VB'\text{-}CB}\rvert^2)$ (D_{VB}/D_{CB})
$(D_{VB}/D_{CB})_{Fc}$	(D_{VB}/D_{CB}) for Fc
$(D_{VB}/D_{CB})_{MnO2}$	(D_{VB}/D_{CB}) for MnO_2
x_0	closest distance of $Na^+_{(sf)}$ to Fc or $Li^+_{(sf)}$ to MnO_2
p, *p*-value	stoichiometric coefficient, number of $Na^+_{(sf)}$ or $Li^+_{(sf)}$ available for adsorption
$(p_{Fc})_{max}$	maximum number of $Na^+_{(sf)}$ adsorption onto Fc
$(p_{MnO_2})_{max}$	maximum number of $Li^+_{(sf)}$ adsorption onto MnO_2
(S_{Fc}/S_{Na+})	the ratio of Fc total surface area for $2x_0$ extended unit crystal lattice to the circle area in Na^+ radius
(S_{MnO_2}/S_{Li^+})	the ratio of MnO_2 total surface area for $2x_0$ extended unit crystal lattice to the circle area in Li^+ radius
f_S	fraction ratio of the area actually occupied by $Na^+_{(sf)}$ or $Li^+_{(sf)}$ on adsorption surface
f_P	1- (porosity, %, of positive active materials)/100
N_{Fc}	number of Fc in the unit crystal lattice
N_{Mn}	number of Mn in the unit crystal lattice
F	the Faraday constant
$(M_{Fc})_{eff}$	effective molality of Fc
$(M_{Fc})_{mes}$	measured molality of Fc
$(M_{MnO_2})_{eff}$	effective molality of MnO_2
$(M_{MnO_2})_{mes}$	measured molality of MnO_2
λ	utilization coefficient
λ_{Fc}	Fc utilization coefficient, $(M_{Fc})_{eff}/(M_{Fc})_{mes}$
λ_{MnO_2}	MnO_2 utilization coefficient, $(M_{MnO_2})_{eff}/(M_{MnO_2})_{mes}$
q	number of cubic or rectangular unit blocks to examine λ
$(Q_{max})_{(Na\text{-}Fc)}$	measured maximum discharge capacity of Na-Fc positive electrode
$(Q_{max})_{(Li\text{-}MnO_2)}$	measured maximum discharge capacity of Li-MnO_2 positive electrode

Introduction

The specific capacity 3860 mAh/g of Li is more than 10 times higher than that of lithium-ion battery positive electrodes, and alkali metal rechargeable batteries are expected to be the next-generation energy device. In order to take advantage of the high specific capacity of alkali metals, it is necessary to develop cathode-active materials with high specific capacity. Sulfur, which has a specific capacity of 1670 mAh/g, more than six times that of lithium-ion positive electrodes, is one of the candidates for future cathode active materials [1].

In 2017, Braga *et al*. presented three types of batteries of Li-S, Na-Fc, and Li-MnO_2, which employed newly developed glass solid electrolytes（$Li_{2.99}Ba_{0.005}O_{1+x}Cl_{1-2x}$ or $Na_{2.99}Ba_{0.005}O_{1+x}Cl_{1-2x}$） [2]. In all of these batteries, alkali metal deposition in the positive active materials during battery discharge was observed, which was a difficult battery phenomenon to understand [3]. Among these three types of batteries, Li-S was reported in the most detail, and its capacity was over 10 times the theoretical capacity of S_8 in the positive active materials. The emergence of these batteries was considered the forerunner of a paradigm-shifting battery phenomenon that was not an extension of conventional battery development concepts. These battery phenomena should reaffirm their importance and attractiveness in the future development of all-solid-state rechargeable batteries with alkali metal anodes. Needless to say, a detailed reaction mechanism for these battery phenomena is essential for their proper design as practical batteries. However, at the time, an electrochemical reaction mechanism relating to these battery phenomena was unknown [2-6].

One of the main reasons for the lack of understanding of the cathode reactions in Braga-Goodenough batteries seems to be the lack of analysis from a cross-disciplinary perspective, such as chemistry, electrochemistry, solid-state physics, and heterojunction physics [7]. Different fields of expertise generally have different perspectives of analysis. However, as the same battery reactions are observed, the results of the analyses of the reaction mechanisms examined from the perspective of the respective disciplines are considered to contain elements that complement each other. Therefore, it is considered that there are common elements that allow results on reaction mechanisms from the viewpoints of chemistry and electrochemistry to share rationality with results on reaction mechanisms from the viewpoints of solid-state and heterojunction physics [8].

The alkali metal deposition reaction is usually written as $Li^+ + e \rightarrow Li$, taking the lithium deposition reaction as an example. However, it is clear that this reaction does not proceed in the cathode potential range [3]. For alkali metal deposition to occur at the cathodes as spontaneous reactions, the electron energy levels of the Na^+gl^- and Li^+gl^- alkali metal ions in the positive active materials must be lower than those of the alkali metal ions in the anode active materials. In other words, the condition for $\Delta G < 0$ with regard to the Gibbs' free energy change of the reaction systems is that the electron energy levels of the alkali metal ions in the positive active materials must be lower than those of the alkali metal ions in the anode active materials. That is, the Na^+gl^- and Li^+gl^- alkali metal ions in the positive active materials and the alkali metal ions in the anode active materials are chemically different. On the basis of the experimental results of Braga *et al.* [2], the electron energy levels of alkali metal ions in the Na^+gl^- and Li^+gl^- surface states in the positive active materials are considered to be lowered to the electron energy levels of Fc and MnO_2, the potential-determining materials of the positive electrodes.

Adsorption as chemisorption is a possible cause of this significant change in the electron energy levels [9-12]. The major difference between the active materials of the cathodes and those of the anodes is the presence of Fc and MnO_2 in the positive active materials and the absence of those in the negative active materials. Therefore, Na^+gl^- and Li^+gl^- alkali metal ions in the positive active

materials are considered to be in a state where molecular orbital contact is possible through solid/solid contact with Fc and MnO_2, and the adsorption by this molecular orbital contact is expected to lower the electron energy levels of the alkali metal ions to the electron energy level region of Fc and MnO_2.

Na^+gl^- and Li^+gl^- are insulators [2], Fc and MnO_2 are semiconductors [13,14]. From the perspective of solid-state and heterojunction physics, these solid/solid contact interfaces are regions such as Schottky barriers and band discontinuities. In recent years, the theory of generalized charge neutrality level, ϕ^G_{CNL}, [15-25] (see Appendix), has made it possible to analyze the electron energy levels of these solid/solid contact interfaces in consideration of orbital hybridization. The cathode reaction mechanisms of Na-Fc and Li-MnO_2 proposed in this paper are based on these backgrounds and disclose the deposition mechanisms of alkali metals at the positive electrodes.

In the previous paper [8], Li-S was first focused on, and its electrochemical reaction mechanism was investigated by employing ϕ^G_{CNL}. In this paper, the electrochemical reaction mechanisms of the other two batteries of Na-Fc and Li-MnO_2 were also investigated by employing ϕ^G_{CNL} on the basis of the facts from the experiments of Braga *et al*. [2], and two new types of mechanisms for Na-Fc and Li-MnO_2 were proposed.

Li-MnO_2 shows two possible mechanisms. One is the same mechanism as Na-Fc, where $Na^+_{(sf)}$ and $Li^+_{(sf)}$ adsorb one-to-one onto Fc and MnO_2 in the positive active materials, respectively. Another mechanism of Li-MnO_2 is the simultaneous adsorption of two $Li^+_{(sf)}$ onto MnO_2. In both reaction mechanisms for Na-Fc and Li-MnO_2, the deposition of alkali metals is caused by intramolecular electron transfer reactions within adsorbed molecules formed by orbital hybridization at heterojunction interfaces. These mechanisms proposed in this paper reflect the relationship between orbital hybridization at heterojunction interfaces and intramolecular electron transfer reactions, taking account of the ϕ^G_{CNL} analysis and its consistency with the facts from the experiments of Braga *et al*. [2]. The two mechanisms of Li-MnO_2 were also analyzed using ϕ^G_{CNL} to determine which mechanism is the thermodynamically dominant. ϕ^G_{CNL} has served to provide significant criteria for examining these reaction mechanisms in terms of solid-state and heterojunction physics. These reaction mechanisms are analyzed in a manner complementary to chemistry, electrochemistry, solid-state physics, and heterojunction physics.

On the basis of these mechanisms, the maximum alkali metal deposition and maximum discharge capacity of Na-Fc and Li-MnO_2 positive electrodes were investigated and found to be determined by the effective number of contacts that allow orbital hybridization between $Na^+_{(sf)}$ and Fc and $Li^+_{(sf)}$ and MnO_2 and the effective molality of Fc and MnO_2 in the positive active materials. The discharge capacity of these batteries is expected to be about 14 times that of the Na-Fc cathode and about 17 times that of the Li-MnO_2 cathode under the conditions considered herein.

In this paper, these reaction mechanisms are presented in detail, and based on these mechanisms, the cathode alkali metal deposition and discharge capacity of Na-Fc and Li-MnO_2 are investigated in detail.

Experimental

In this paper, all experimental results for Na-Fc and Li-MnO_2 are taken from the data and descriptions in Braga *et al*. [2]. The reaction mechanisms of these batteries are essentially based on the facts [2] that Na and Li are deposited on the positive electrode during the discharge of Na-Fc and Li-MnO_2, respectively.

Results and discussion

A C[(CE)cC]n model for Na-Fc and Li-MnO_2

Figure 1 shows the Braga-Goodenough Na-Fc and Li-MnO_2 battery diagram. These positive active materials consist of Na^+gl^- powder, Fc powder, carbon black powder, and Cu current collector for Na-Fc, and Li^+gl^- powder, MnO_2 powder, carbon black powder, and Cu current collector for Li-MnO_2. At the interfaces between the potential-determining materials Fc and MnO_2 and these glass solid electrolyte powders, Na for Na-Fc and Li for Li-MnO_2 are deposited in the positive active materials during discharge [2].

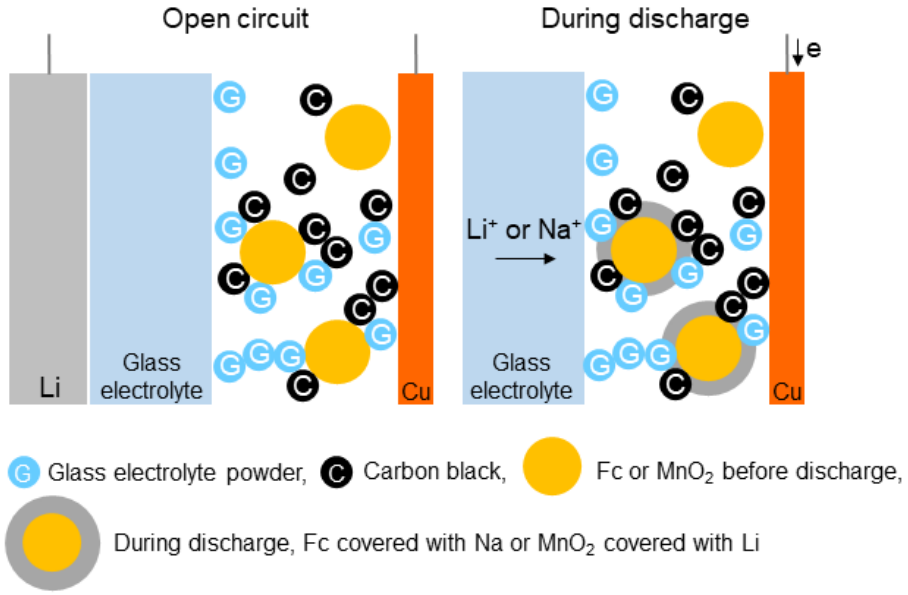

Figure 1. *Diagrams of positive electrode active materials reflecting the C[(EC)cC]n mechanism on the Braga-Goodenough Na-Fc and Li-MnO_2 battery under open circuit and discharge conditions*

In ordinary battery terminology, for Na-Fc and Li-MnO_2, the cathode corresponds to the positive electrode, and the anode corresponds to the negative electrode. In this paper, however, since the phenomenon of alkali metal deposition on the cathode during battery discharge is confined to Braga-Goodenough batteries, these terms are often used together to clarify the battery phenomenon.

In the case of Na-Fc, one type of reaction mechanism of the positive electrode is considered. On the other hand, in the case of Li-MnO_2, two types of mechanisms are considered to be possible. One is the one-to-one adsorption of $Li^+_{(sf)}$ onto MnO_2, which is the same case as $Na^+_{(sf)}$ onto Fc. The other is that two $Li^+_{(sf)}$ adsorb simultaneously onto MnO_2. In this section, the case of the same mechanism in Na-Fc and Li-MnO_2 is examined, using mainly the notation in Na-Fc. The other mechanism for Li-MnO_2 will be discussed in the next section.

Eqs. (1) to (10) are the elementary reactions of Na-Fc cathode discharge. The first step, Eq. (1) shows the adsorption equilibrium reaction. The left side of Eq. (1) shows that $p\mathrm{Na}^+_{(sf)}$ for one Fc will occupy the position where orbital hybridization is possible due to the contact between Fc and Na^+gl^-. The right side of Eq. (1) indicates that among these $p\mathrm{Na}^+_{(sf)}$, one $Na^+_{(sf)}$ with the highest probability of orbital hybridization at the interface with Fc forms the adsorbed molecule of $\mathrm{Fc}[\mathrm{Na}^+_{(sf)}(\mathrm{ad})](p\text{-}1)(\mathrm{Na}^+_{(sf)})$. The remaining $(p\text{-}1)\mathrm{Na}^+_{(sf)}$ are in a waiting state because Fc is already used for one adsorption bond. Here, the stoichiometric coefficient p is an integer, $p \geq 1$. In this paper, terms related to adsorption, such as adsorption equilibrium reactions, are based on orbital hybridization at the heterojunction interfaces.

Fc is a stable metallocene with Fe(II) as the center and cyclopentadienyl as the upper and lower sandwich structure. Fc has Fe(II) $3d_{z2}$, $3d_{xy}$, and $3d_{x2-y2}$ orbitals in the valence band and $3d_{xz}$ and $3d_{yz}$ orbitals in the conduction band [13]. Fc^+/Fc shows a typical reversible voltammogram in organic solvents, and its redox center is at Fe(II). This is a one-electron redox reaction on the 3d orbital, and Eq. (1) is also considered to involve the 3d orbital.

Assuming that Eqs. (2), (3) and (4) are a set of reactions related to Na deposition, the discharge reaction proceeds by repeating this set of reactions with the *p*-value decreasing by one after reaction Eq. (5). If the number of cycles of this set of reactions is *n*, the n^{th} Na deposition occurs in the nth cycle. Then at the end of the n^{th} cycle, the amount of discharge electricity and Na deposition of the positive electrode are *nF* (C) and *n* moles, respectively, where *n* is an integer $n \le p$. Since the first and the second set of reactions correspond to Eqs. (2) to (4) and Eqs. (5) to (7), respectively, the following Eqs. (8) to (10) correspond to the *n*th set of reactions.

$$Fc + p{Na^+}_{(sf)} \leftrightarrow Fc\,[{Na^+}_{(sf)}\,(ad)]\,(p\text{-}1)({Na^+}_{(sf)}) \quad (1)$$

$$Fc\,[{Na^+}_{(sf)}\,(ad)]\,(p\text{-}1)({Na^+}_{(sf)}) \rightarrow Fc^+\,Na\,(p\text{-}1)({Na^+}_{(sf)}) \quad (2)$$

$$Fc^+\,Na\,(p\text{-}1)({Na^+}_{(sf)}) + e \rightarrow Fc\,Na\,(p\text{-}1)({Na^+}_{(sf)}) \quad (3)$$

$$Fc\,Na\,(p\text{-}1)({Na^+}_{(sf)}) \leftrightarrow Fc\,[{Na^+}_{(sf)}\,(ad)]\,Na\,(p\text{-}2)({Na^+}_{(sf)}) \quad (4)$$

$$Fc\,[{Na^+}_{(sf)}\,(ad)]\,Na\,(p\text{-}2)({Na^+}_{(sf)}) \rightarrow Fc^+\,2Na\,(p\text{-}2)({Na^+}_{(sf)}) \quad (5)$$

$$Fc^+\,2Na\,(p\text{-}2)({Na^+}_{(sf)}) + e \rightarrow Fc\,2Na\,(p\text{-}2)({Na^+}_{(sf)}) \quad (6)$$

$$Fc\,2Na\,(p\text{-}2)({Na^+}_{(sf)}) \leftrightarrow Fc\,[{Na^+}_{(sf)}\,(ad)]\,2Na\,(p\text{-}3)({Na^+}_{(sf)}) \quad (7)$$

$$Fc\,[{Na^+}_{(sf)}\,(ad)]\,(n\text{-}1)Na\,(p\text{-}n)({Na^+}_{(sf)}) \rightarrow Fc^+\,nNa\,(p\text{-}n)({Na^+}_{(sf)}) \quad (8)$$

$$Fc^+\,nNa\,(p\text{-}n)({Na^+}_{(sf)}) + e \rightarrow Fc\,nNa\,(p\text{-}n)({Na^+}_{(sf)}) \quad (9)$$

$$Fc\,nNa\,(p\text{-}n)({Na^+}_{(sf)}) \leftrightarrow Fc\,[{Na^+}_{(sf)}\,(ad)]\,nNa\,(p\text{-}n\text{-}1)({Na^+}_{(sf)}) \quad (10)$$

Eq. (2) is the intramolecular electron transfer reaction of the adsorbed molecule. In Eq. (2), Fc reduces $[{Na^+}_{(sf)}\,(ad)]$ in the $Fc[{Na^+}_{(sf)}(ad)](p\text{-}1)({Na^+}_{(sf)})$ in the one-electron transfer reaction and is itself oxidized to deposit Na as $Fc^+Na(p\text{-}1)({Na^+}_{(sf)})$. Eq. (3) is the electrochemical reaction in which Fc^+ of the $Fc^+Na(p\text{-}1)({Na^+}_{(sf)})$ generated in Eq. (2) receives one electron from the Na negative electrode and immediately returns to the original Fc to form $FcNa(p\text{-}1)({Na^+}_{(sf)})$. Eq. (4) is the adsorption equilibrium reaction that produces the new adsorbed molecule $Fc[{Na^+}_{(sf)}(ad)]Na(p\text{-}2)({Na^+}_{(sf)})$ from $FcNa(p\text{-}1)({Na^+}_{(sf)})$ produced in Eq. (3). At this time, one ${Na^+}_{(sf)}$ with the highest probability of orbital hybridization from $(p\text{-}1)({Na^+}_{(sf)})$ forms the new adsorption bond orbital of $Fc[{Na^+}_{(sf)}(ad)]Na(p\text{-}2)({Na^+}_{(sf)})$.

In this paper, this mechanism is denoted as C[(CE)cC]*n*, where C denotes the chemical reaction step, and E denotes the electrochemical reaction step. The c in (CE)cC denotes that the (CE)c is catalytic reaction steps. Here, the intramolecular electron transfer reaction of the adsorbed molecule is denoted as a chemical reaction because it does not appear as an external current. The catalytic function is performed by Fc for Na-Fc. The *n* in C[(CE)cC]*n* indicates that the set of reactions of this [(CE)cC] part will cycle *n* times. Therefore, for $n = p$, the cycle is maximized. Under $n = p$ conditions, the [(CE)cC] cycle process terminates at the (CE)c, and the subsequent C, the adsorption equilibrium reaction, disappears because all $p{Na^+}_{(sf)}$ on Fc are discharged and reduced to *p*Na and there is no ${Na^+}_{(sf)}$ available for adsorption on Fc. The step of the deposition of Na corresponds to the step C in the (CE)c.

The intramolecular electron transfer of the adsorbed molecule in Eqs. (2), (5) and (8) results in Fc becoming Fc^+, which is ascribed to the one-electron transfer from the *d* orbital of the valence band of Fe(II) of Fc to ${Na^+}_{(sf)}(ad)$. The open circuit voltage of Na-Fc is about 2.3 volts as read from the

charge-discharge cycle data [2], and the significant figures would be two digits at most. As described above, Fc^+ is immediately reduced and returned to Fc in the subsequent E step by Eqs. (3), (6), (9) and Fc consequently undergo no apparent change. In Eqs. (1) to (10), the currents observed externally correspond to the currents in these electrochemical reactions Eqs. (3), (6) and (9).

On discharge, Fc contacts the electron energy of the Na negative electrode, whose electron level is about 2.3 eV higher than the Fermi level of Fc, *via* the current collectors. That is, Fc is in an electrochemical reaction condition where the overpotential is greatly superimposed on the negative side, and Fc^+ is immediately reduced to Fc, with a large reaction rate expected in this E step. The catalytic reactions of Fc regarding the Na deposition in the positive active materials correspond to be the second C and the subsequent E steps in the C[(CE)cC]*n* mechanism. The intramolecular electron transfer reaction corresponding to the second C in the C[(CE)cC]*n* mechanism will be further discussed together with the case of Li-MnO_2 in the section of the orbital hybridization and charge transfer at heterojunction interfaces in terms of ϕ^G_{CNL}.

The total reaction equation for the (CE)c part at $n = p$, *i.e.* the maximum number of cycles, is the sum of Eqs. (8) and (9), resulting in the following Eq. (11), and the C[(CE)cC]*n* mechanism terminates at the E step of Eq. (9), as described above. Here, at $n = p$, the terms of $Fc[Na^+_{(sf)}(ad)](n\text{-}1)Na$ $(p\text{-}n)(Na^+_{(sf)})$, $Fc^+nNa(p\text{-}n)(Na^+_{(sf)})$, and Fc $nNa(p\text{-}n)(Na^+_{(sf)})$ in Eqs. (8) and (9) become $Fc[Na^+_{(sf)}(ad)]$ $(p\text{-}1)Na$, Fc^+pNa, and Fc pNa, respectively.

$$Fc\ [Na^+_{(sf)}\,(ad)]\ (p\text{-}1)Na + e \rightarrow Fc\ pNa \tag{11}$$

In comparing Eqs. (8), (9), and (11), it is clear that the elementary reactions of Fc as a catalyst correspond to Eqs. (8) and (9) in the (CE)c part of the C[(CE)cC]*n* mechanism.

Eq. (12) is the overall reaction of the positive electrode, which is obtained from the sum of Eqs. (1) through (10).

$$Fc + pNa^+_{(sf)} + ne \rightarrow Fc\ [Na^+_{(sf)}\,(ad)]\ nNa\ (p\text{-}n\text{-}1)(Na^+_{(sf)}\,) \tag{12}$$

Eq. (12) involves the general case for $n < p$. At $n = p$, Eq. (12) demonstrates the maximum number of cycles, as described above, and Eq. (10) disappears, so that the overall reaction for the positive electrode is Eq. (13) from the sum of Eqs. (1) through (9). Eq. (13) is also obtained from Eq. (12) as $n = p$.

$$Fc + pNa^+_{(sf)} + pe \rightarrow Fc\ pNa \tag{13}$$

In the battery overall reaction, the Na negative electrode reactions, which are paired with the overall reaction of the positive electrode in Eq. (12), are Eqs. (14) and (15) as follows:

$$nNa \rightarrow nNa^+ + ne \tag{14}$$

$$nNa^+ \leftrightarrow nNa^+_{(sf)} \tag{15}$$

The overall reaction of the Na anode is Eq. (16) from the sum of Eqs. (14) and (15) as follows:

$$nNa \rightarrow nNa^+_{(sf)} + ne \tag{16}$$

Therefore, the overall battery reaction of Na-Fc is Eq. (17) from the sum of Eqs. (12) and (16) as follows:

$$Fc + (p\text{-}n)Na^+_{(sf)} + nNa \rightarrow Fc\ [Na^+_{(sf)}\,(ad)]\ nNa\ (p\text{-}n\text{-}1)(Na^+_{(sf)}\,) \tag{17}$$

When $n = p$, Eq. (17) is equal to Eq. (18), which is also obtained from the sum of Eq. (13) for the positive electrode and Eq. (16) for the negative electrode.

$$Fc + pNa \rightarrow Fc\ pNa \tag{18}$$

The charging reaction of this C[(CE)cC]*n* mechanism corresponds to the reverse reaction of this mechanism. Under charge-discharge cycle conditions, it is unlikely that $Na^+_{(sf)}$ and $Li^+_{(sf)}$ after

charging are the same as before discharging. It is natural to assume that the stoichiometric coefficient *p*-value appearing in Eq. (1) can change from cycle to cycle.

Regarding Na-Fc charge-discharge cycle tests [2], the data are demonstrated to 200 cycles, corresponding to 33.3 days. 100th cycle discharge and charge voltages overlap when compared to those of the 200th cycle, and there is no degradation of charge-discharge characteristics between 100 and 200 cycles. These charge-discharge cycle characteristics of Na-Fc are considered to be ascribed to the sustainability of the C[(CE)cC]*n* mechanism during charge-discharge cycling.

In the case of Li-MnO_2, the notations of Eqs. (1) to (18) of the C[(CE)cC]*n* mechanism for Li-MnO_2 can be expressed by changing the notations from Na-Fc to Li-MnO_2, where Fc is replaced by MnO_2, intermediate Fc^+ by intermediate $Mn(O_2)^+$, Na by Li, and $Na^+_{(sf)}$(ad) by $Li^+_{(sf)}$(ad). Eq. (1) is the adsorption equilibrium reaction resulting from the contact between MnO_2 and Li^+gl^-. Eqs. (1) to (10) relate to the adsorption equilibrium reactions of one $Li^+_{(sf)}$ to MnO_2. The valence band of MnO_2 is composed of oxygen O^{2-}, and its conduction band is composed of Mn(IV) [20]. MnO_2 involves two O^{2-} 2p orbitals per Mn, and Eq. (1) for Li-MnO_2 shows that one $Li^+_{(sf)}$ is capable of adsorbing one of these O^{2-} 2p orbitals. MnO_2 becomes $Mn(O_2)^+$ by the intramolecular electron transfer of the adsorbed molecule in Eqs. (2), (5), and (8). $Mn(O_2)^+$ does not appear in the overall reaction equations of the positive electrode as Fc^+ does. $Mn(O_2)^+$ is immediately reduced to MnO_2 for the same reason as Fc^+, according to Eqs. (3), (6), and (9): the Li anode potential is about 3 volts lower than the Li-MnO_2 cathode because the open circuit voltage [2] of Li-MnO_2 is about 3.0 volts. The notation $Mn(O_2)^+$ is considered to be appropriate for Eqs. (2), (5) and (8) in the sense that the oxygen anion $2O^{2-}$ in MnO_2 is the side that donates one electron to $Li^+_{(sf)}$. The catalytic reactions of MnO_2 on Li deposition correspond to be the second C and the subsequent E steps, *i.e.* (CE)c steps, in the C[(CE)cC]*n* mechanism as well as Na-Fc.

Eq. (19) from Eq. (12) is the overall reaction of the positive electrode of Li-MnO_2, and Eq. (20) from Eq. (17) is the overall battery reaction of Li-MnO_2.

$$MnO_2 + pLi^+_{(sf)} + ne \rightarrow MnO_2\,[Li^+_{(sf)}\,(ad)]\;nLi\;(p\text{-}n\text{-}1)(Li^+_{(sf)}) \quad (19)$$

$$MnO_2 + (p\text{-}n)Li^+_{(sf)} + nLi \rightarrow MnO_2\,[Li^+_{(sf)}\,(ad)]\;nLi\;(p\text{-}n\text{-}1)(Li^+_{(sf)}) \quad (20)$$

At $n = p$ for the maximum number of cycles, the overall reaction of the positive electrode is Eq. (21) from Eq. (13) or Eq. (19). The battery overall reaction is Eq. (22) from Eq. (18) or Eq. (20) as $n = p$.

$$MnO_2 + pLi^+_{(sf)} + pe \rightarrow MnO_2\,pLi \quad (21)$$

$$MnO_2 + pLi \rightarrow MnO_2\,pLi \quad (22)$$

Not only Fc but also Mn(IV) in MnO_2 is not changed in this mechanism, which is also supported by the charge-discharge cycle tests, which were conducted under various charge and discharge time conditions for up to 270 cycles for a total of 112.5 days [2]. In these tests, no degradation of charge-discharge characteristics was observed until the test was terminated on day 112.5. If Mn(III) is formed, like a primary battery of lithium manganese dioxide, on discharge, the charge-discharge cycle characteristics will gradually deteriorate, and cycle tests will not continue.

In respect of the electron energy levels of adsorbed particles, in general, they are not the same as those of isolated ones [9-12]. In the C[(CE)cC]*n* mechanism, $Na^+_{(sf)}$ forms the adsorption bond with Fc which significantly lowers $Na^+_{(sf)}$ electron energy level. The electron energy level of $Na^+_{(sf)}$ decreases from the LUMO level of $Na^+_{(sf)}$ to the electron energy level region of Fc as $Na^+_{(sf)}$ approaches Fc, while gradually broadening its level width [9,12].

Figure 2 shows that the electron energy levels of $Na^+_{(sf)}$ vary significantly with distance from Fc. The relationship between MnO_2 and $Li^+_{(sf)}$ can be drawn similarly. The electron energy level width

reaches its maximum at a distance of x_0 from Fc where orbital hybridization is possible [12]. At the same time, the adsorption energy curve, ΔG_{ad}, becomes the most stable energy state [9,12]. Therefore, the position of $p\mathrm{Na}^{+}_{(sf)}$ in Eq. (1) is in this x_0 region. The x_0 on the x-axis in Figure 2 is considered to be around 200 pm (0.2 nm) level, as shown in the following consideration. This value x_0 is one of the essential points in determining the maximum number of cycles of the deposition of alkali metals in the positive active materials and the maximum discharge capacity of Na-Fc and Li-MnO_2 positive electrodes, as will be described in other sections.

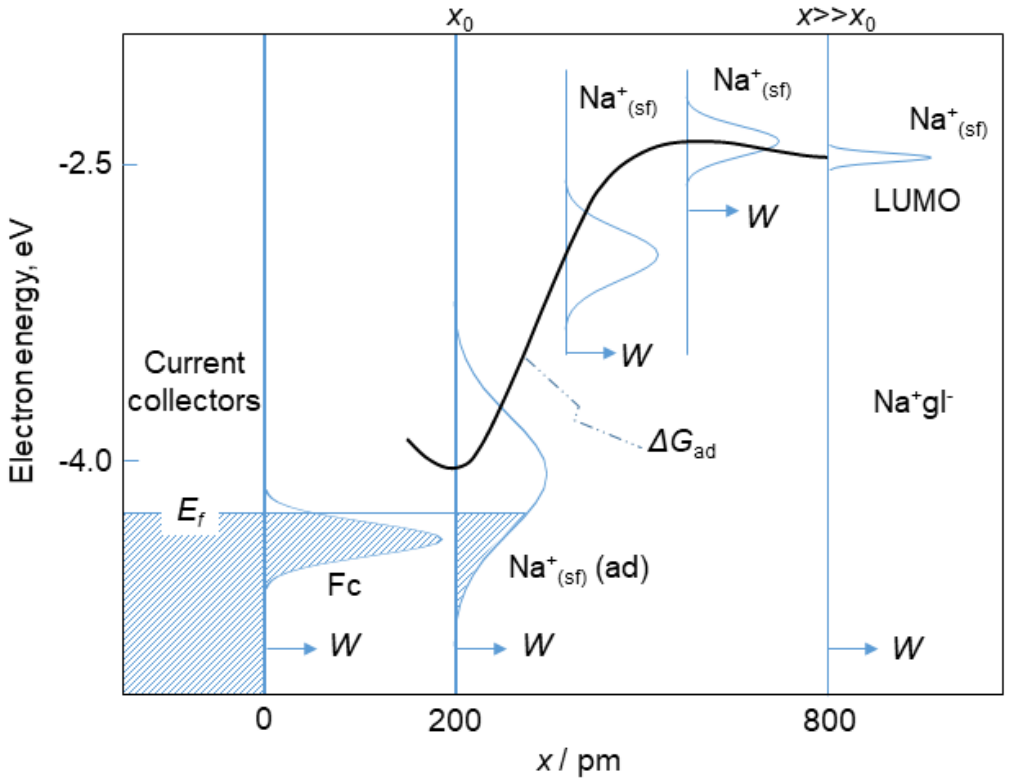

Figure 2. *Variation of electron energy levels of $Na^{+}_{(sf)}$ adsorbates at various distances from the adsorbent Fc surface. As $Na^{+}_{(sf)}$ approaches Fc, the electron energy levels of $Na^{+}_{(sf)}$ spread out due to its interaction with Fc, having the widest probability density at x_0 of the G_{ad} minimum. ΔG_{ad} = adsorption energy curve of $Na^{+}_{(sf)}$ approaching Fc,* W *= probability density of electron energy states,* x *= distance to $Na^{+}_{(sf)}$, and x_0 = distance to adsorbed $Na^{+}_{(sf)}$ (ad)*

In the solution-based electric double layer, the inner Helmholtz layer is 200 pm and the outer Helmholtz layer is 300 pm [21]. The inner Helmholtz layer is the region of inner-sphere electron transfer, where reaction species are desolated, and the orbital hybridization and adsorption behavior between reaction species and electrode materials become apparent. Therefore, the inner-sphere electron transfer is clearly distinguished from the electron transfer reaction in the outer Helmholtz layer, *i.e.* outer-sphere electron transfer, where orbital hybridization between reaction species and electrode materials is not easy perceptible. The x_0 shown in Figure 2 is considered equivalent to the position of this inner-sphere electron transfer, which is around 200 pm for Na-Fc and Li-MnO_2. The *y*-axis scale is estimated based on the HOMO level of -4.8 eV for isolated Fc and the open circuit voltage of *ca.* 2.3 volts for Na-Fc. In Figure 2, the shaded region below the E_f indicates the overlap of the electron energy distributions of the current collectors, Fc, and $\mathrm{Na}^{+}_{(sf)}$(ad). The Fermi level, *E*f, of the Cu and carbon black current collectors, coincides with that of $\mathrm{FcNa}^{+}_{(sf)}$(ad) and demonstrates the potential of the positive electrode of Na-Fc under open circuit equilibrium conditions.

With regard to the surface states, $Na^+_{(sf)}$ and $Li^+_{(sf)}$ in the C[(CE)cC]*n* mechanism are denoted with the intention that the electron energy levels of these surface states are different from those of the internal Na^+ of Na^+gl^- and Li^+ of Li^+gl^-. It is clear that $Na^+_{(sf)}$ and $Li^+_{(sf)}$ levels at the Na^+gl^- and Li^+gl^- surfaces, rather than within them, are directly involved in the battery reactions of Na-Fc and Li-MnO_2. In general, in ionic-bonded oxides, the metal ion constitutes the conduction band [20], and the oxygen ion constitutes the valence band [20], even though some of these oxides are partially covalent. The surface states of a metal ion in a metal oxide are basically the electron level of the metal ion, which should be at the level of the conduction band, but whose energy is reduced due to surface effects and shifted into the band gap [22].

Na^+gl^- and Li^+gl^- are amorphous [2,4-6], and their band structures differ from crystalline ones. In the amorphous case, the conduction band bottom E_{CB} in the crystalline case corresponds to the diffuse-band-tail states, a distribution of density of states that decays slowly toward the low energy side [23]. Amorphous structures do not seem to inhibit the C[(CE)cC]*n* mechanism. Rather, it affects the C[(CE)cC]*n* mechanism. Diffuse-band-tail states may be considered to have the effect of dispersing and increasing the surface states in the region below the LUMO level shown in Figure 2. Amorphous structures of Na^+gl^- and Li^+gl^- would enhance the opportunity for orbital hybridization contacts between Fc and $Na^+_{(sf)}$ and MnO_2 and $Li^+_{(sf)}$ at lower energy levels in the C[(CE)cC]*n* mechanism.

A C[2(CE)cC]n model for Li-MnO_2

In the case of Li-MnO_2, the reaction mechanism of the simultaneous adsorption of two $Li^+_{(sf)}$ onto MnO_2 is discussed in this section. The corresponding reaction equations are given in Eqs. (23) to (38) below. This reaction mechanism is denoted as C[2(CE)cC]*n* in this paper. The 2 in the 2(CE)c part means that two consecutive (CE)c steps are involved, and the c in the 2(CE)c part denotes that it is the catalytic reaction part as in the case of the C[(CE)cC]*n* mechanism. The group of reaction equations between the long horizontal lines corresponds to the [2(CE)cC] part in C[2(CE)cC]*n*. The *n* in C[2(CE)cC]*n* indicates that the set of reactions of this [2(CE)cC] part will cycle *n* times.

It is sufficient to elucidate this mechanism when *p* is even because when *p* is odd, adding the C[(CE)cC]*n* mechanism with *p* = 1 will complete the C[2(CE)cC]*n* mechanism. In the following, *p*-values are treated as even numbers.

$$MnO_2 + pLi^+_{(sf)} \leftrightarrow MnO_2\,[2Li^+_{(sf)}\,(ad)]\,(p\text{-}2)(Li^+_{(sf)}) \quad (23)$$

$$MnO_2\,[2Li^+_{(sf)}\,(ad)]\,(p\text{-}2)(Li^+_{(sf)}) \rightarrow Mn(O_2)^+\,[Li^+_{(sf)}\,(ad)]\,Li\,(p\text{-}2)(Li^+_{(sf)}) \quad (24)$$

$$Mn(O_2)^+\,[Li^+_{(sf)}\,(ad)]\,Li\,(p\text{-}2)(Li^+_{(sf)}) + e \rightarrow MnO_2\,[Li^+_{(sf)}\,(ad)]\,Li\,(p\text{-}2)(Li^+_{(sf)}) \quad (25)$$

$$MnO_2\,[Li^+_{(sf)}\,(ad)]\,Li\,(p\text{-}2)(Li^+_{(sf)}) \rightarrow Mn(O_2)^+\,2Li\,(p\text{-}2)(Li^+_{(sf)}) \quad (26)$$

$$Mn(O_2)^+\,2Li\,(p\text{-}2)(Li^+_{(sf)}) + e \rightarrow MnO_2\,2Li\,(p\text{-}2)(Li^+_{(sf)}) \quad (27)$$

$$MnO_2\,2Li\,(p\text{-}2)(Li^+_{(sf)}) \leftrightarrow MnO_2\,[2Li^+_{(sf)}\,(ad)]\,2Li\,(p\text{-}4)(Li^+_{(sf)}) \quad (28)$$

$$MnO_2\,[2Li^+_{(sf)}\,(ad)]\,2Li\,(p\text{-}4)(Li^+_{(sf)}) \rightarrow Mn(O_2)^+\,[Li^+_{(sf)}\,(ad)]\,3Li\,(p\text{-}4)(Li^+_{(sf)}) \quad (29)$$

$$Mn(O_2)^+\,[Li^+_{(sf)}\,(ad)]\,3Li\,(p\text{-}4)(Li^+_{(sf)}) + e \rightarrow MnO_2\,[Li^+_{(sf)}\,(ad)]\,3Li\,(p\text{-}4)(Li^+_{(sf)}) \quad (30)$$

$$MnO_2\,[Li^+_{(sf)}\,(ad)]\,3Li\,(p\text{-}4)(Li^+_{(sf)}) \rightarrow Mn(O_2)^+\,4Li\,(p\text{-}4)(Li^+_{(sf)}) \quad (31)$$

$$Mn(O_2)^+\,4Li\,(p\text{-}4)(Li^+_{(sf)}) + e \rightarrow MnO_2\,4Li\,(p\text{-}4)(Li^+_{(sf)}) \quad (32)$$

$$MnO_2\,4Li\,(p\text{-}4)(Li^+_{(sf)}) \leftrightarrow MnO_2\,[2Li^+_{(sf)}\,(ad)]\,4Li\,(p\text{-}6)(Li^+_{(sf)}) \quad (33)$$

Eq. (23) is the first step, which shows that two $Li^+_{(sf)}$ of the $pLi^+_{(sf)}$ in the region of adsorption position x_0 shown in Figure 2 are adsorbed simultaneously, and the adsorption equilibrium is

established. Eq. (24) is the adsorption intramolecular one electron transfer from O^{2-} in the valence band of MnO_2 to one of $2Li^+_{(sf)}(ad)$, where the MnO_2 side becomes $Mn(O_2)^+$, and one Li is deposited from $2Li^+_{(sf)}$ (ad). This electron transfer does not take current externally. Eq. (25) is the E step in which $Mn(O_2)^+$ produced by the intramolecular electron transfer is immediately reduced to MnO_2 under the potential of the Li anode, as described in the C[(CE)cC]*n* mechanism. Eq. (26) is again the intramolecular electron transfer reaction. So far, one of the two $Li^+_{(sf)}$ in the adsorbed molecule formed in Eq. (23) has already been reduced to Li. Eq. (26) is the reaction in which the remaining $Li^+_{(sf)}$ adsorbed molecule is reduced again by the intramolecular electron transfer, resulting in Li deposition. Eq. (27) is equivalent to Eq. (25), which is the electrochemical reduction of $Mn(O_2)^+$ generated by the intramolecular electron transfer reaction in Eq. (26). Eq. (28) is again the adsorption equilibrium reaction involving two new adsorptions of $Li^+_{(sf)}$.

Assuming that Eqs. (24) to (28) are a set of reactions related to Li deposition, the discharge electricity and Li deposition amount to 2*F* (C) and 2Li, respectively, in this set of reactions. After Eq. (29), this set of reactions is repeated, and the discharge reaction proceeds with the *p*-value ($p \geq 2$) decreasing by two. In the case of $p = 2$ corresponding to the number of cycle $n = 1$, the cycle does not continue and terminates with Eq. (27). The group $n = 1$ is from Eq. (24) up to Eq. (28), and the group $n = 2$ is from Eq. (29) up to Eq. (33). Same as above for $n = 1$, when the cycle terminates with $n = 2$, Eq. (33), which is the third C in the group $n = 2$ disappears as in the case of the C[(CE)cC]*n* mechanism.

The group of reaction equations between short lines and between long and short lines corresponds to the 2(CE)c part in C[2(CE)cC]*n*. That is the pair of Eqs. (24) and (25) and the pair of Eqs. (29) and (30) correspond to the first (CE)c part in 2(CE)c, while the pair of Eqs. (26) and (27) and the pair of Eqs. (31) and (32) correspond to the second (CE)c part in 2(CE)c. The first C in C[2(CE)cC]*n* is Eq. (23), and the third C corresponds to Eqs. (28) and (33). Since Eqs. (24) to (28) correspond to cycle $n = 1$ and Eqs. (29) to (33) correspond to cycle $n = 2$, the reaction equation set for cycle *n* is the following Eqs. (34) to (38).

$$MnO_2\ [2Li^+_{(sf)}(ad)]\ (2n\text{-}2)Li\ (p\text{-}2n)(Li^+_{(sf)}) \rightarrow Mn(O_2)^+\ [Li^+_{(sf)}(ad)]\ (2n\text{-}1)Li\ (p\text{-}2n)(Li^+_{(sf)}) \quad (34)$$

$$Mn(O_2)^+\ [Li^+_{(sf)}(ad)]\ (2n\text{-}1)Li\ (p\text{-}2n)(Li^+_{(sf)}) + e \rightarrow MnO_2\ [Li^+_{(sf)}(ad)]\ (2n\text{-}1)Li\ (p\text{-}2n)(Li^+_{(sf)}) \quad (35)$$

$$MnO_2\ [Li^+_{(sf)}(ad)]\ (2n\text{-}1)Li\ (p\text{-}2n)(Li^+_{(sf)}) \rightarrow Mn(O_2)^+\ 2nLi\ (p\text{-}2n)(Li^+_{(sf)}) \quad (36)$$

$$Mn(O_2)^+\ 2nLi\ (p\text{-}2n)(Li^+_{(sf)}) + e \rightarrow MnO_2\ 2nLi\ (p\text{-}2n)(Li^+_{(sf)}) \quad (37)$$

$$MnO_2\ 2nLi\ (p\text{-}2n)(Li^+_{(sf)}) \leftrightarrow MnO_2\ [2Li^+_{(sf)}(ad)]\ 2nLi\ (p\text{-}2n\text{-}2)(Li^+_{(sf)}) \quad (38)$$

The overall reaction of the positive electrode is Eq. (39) derived by the sum of Eqs. (23) through (38). The battery's overall reaction, including the negative electrode reactions, is derived by the same procedure as the C[(CE)cC]*n* mechanism.

$$MnO_2 + pLi^+_{(sf)} + 2ne \rightarrow MnO_2\ [2Li^+_{(sf)}(ad)]\ 2nLi\ (p\text{-}2n\text{-}2)(Li^+_{(sf)}) \quad (39)$$

The maximum number of cycles is when $n = p/2$, and all $pLi^+_{(sf)}$ is used for discharge. The reaction terminates with Eq. (37), and Eq. (40) of this overall reaction of the positive electrode is obtained from the sum of the reactions in Eqs. (23) to (37), obtained from Eq. (39) as $n = p/2$.

$$MnO_2 + pLi^+_{(sf)} + pe \rightarrow MnO_2\ pLi \quad (40)$$

At $n = p/2$, the terms of $2nLi\ (p\text{-}2n)(Li^+_{(sf)})$ in Eq. (37) and $[2Li^+_{(sf)}(ad)]\ 2nLi\ (p\text{-}2n\text{-}2)(Li^+_{(sf)})$ in Eq. (39) are equal to *p*Li. Eq. (40) becomes Eq. (41) in the case of cycle $n = 1$ corresponding to $p = 2$.

$$MnO_2 + 2Li^+_{(sf)} + 2e \rightarrow MnO_2\ 2Li \quad (41)$$

When *p* is odd, $pLi^+_{(sf)}$ decrease by two, and the positive electrode reaction terminates once at the C[2(CE)cC]*n* mechanism. Consequently, one $Li^+_{(sf)}$ remains as $MnO_2Li^+_{(sf)}(ad)$. This further discharge reaction of $MnO_2Li^+_{(sf)}(ad)$ proceeds by the C[(CE)cC]*n* mechanism. In Eqs. (1) to (3) in the

C[(CE)cC]*n* mechanism, replacing Fc with MnO_2, the intermediate Fc^+ with the intermediate $Mn(O_2)^+$, Na with Li, and $Na^+_{(sf)}$(ad) with $Li^+_{(sf)}$(ad), the overall reaction for the remaining one $Li^+_{(sf)}$ becomes the following Eq. (42).

$$MnO_2 + Li^+_{(sf)} + e \rightarrow MnO_2\ Li \quad (42)$$

Therefore, when *p* is odd, the amount of the positive electrode discharge electricity and Li deposition correspond to the addition of 1*F* (C) and 1 mole to the amount of the discharge electricity of 2*nF* (C) and 2*n* moles of Li deposition when *p* is even in the C[2(CE)cC]*n* mechanism. Eq. (21) in the C[(CE)cC]*n* mechanism is consistent with Eq. (41) when *p* = 2 and with the combined result of Eqs. (41) and (42) when *p* = 3. Therefore, regardless of whether *p* is odd or even, the discharge result of the C[2(CE)cC]*n* mechanism is consistent with that for *n* = *p* in the C[(CE)cC]*n* mechanism. As a result, the discharge results for Li-MnO_2 are the same for both C[2(CE)cC]*n* and C[(CE)cC]*n* mechanisms, although their elementary reactions are different.

Orbital hybridization and charge transfer at heterojunction interfaces in terms of ϕ^G_{CNL}

In this section, interfacial reactions at heterojunction interfaces are examined from the viewpoint of heterojunction physics. In the previous paper [7], the theory of the generalized charge neutrality level, ϕ^G_{CNL}, was applied to analyze the reaction mechanism of the Braga-Goodenough Li-S battery (see Appendix). ϕ^G_{CNL} is also applied here to analyze the reaction mechanisms of the C[(CE)cC]*n* and C[2(CE)cC]*n*. The main points of this section are as follows:

1. Intramolecular electron transfer appearing in the mechanisms is from which orbital to which orbital the electron transfer occurs. This investigation is to reveal the possibility of alkali metal deposition in ϕ^G_{CNL} view.
2. Whether adsorption processes and intramolecular electron transfer reactions by orbital hybridization are compatible with ϕ^G_{CNL} analysis.
3. Which of the two reaction mechanisms in Li-MnO_2 is more likely to proceed thermodynamically in terms of ϕ^G_{CNL}.

This symbol ϕ^G_{CNL} has two meanings [8]: one is the theory itself and the other is the charge neutrality level itself evaluated by ϕ^G_{CNL}.

Initially, ϕ^G_{CNL} views on the directions of electron transfer within adsorbed molecules are shown. ϕ^G_{CNL} shows two possible directions [15-19] of electron transfer at a heterojunction interface as follows:

With respect to Na-Fc, Figure 3 shows the possibilities for the directions of electron transfer based on ϕ^G_{CNL}. Two possibilities for the electron transfer within adsorbed molecules $FcNa^+_{(sf)}$(ad) are shown here. One is the electron transfer from the valence band of Fc to the $Na^+_{(sf)}$ conduction band of Na^+gl^-. The other is the electron transfer from the O^{2-} and Cl^- valence bands of Na^+gl^- to the Fc conduction band.

In the former case, it is consistent with the experimental fact of Braga *et al*. [2] that Na is deposited. Therefore, the electron transfer within adsorbed molecules $FcNa^+_{(sf)}$(ad) is from the valence band of Fc to the conduction band of $Na^+_{(sf)}$, as shown by the bold line in Figure 3. As described in the C[(CE)cC]*n* mechanism, the valence band and conduction band of Fc correspond to those of the splitting of the d-orbitals of Fe(II) at the center of Fc in the ligand field [13]. Na^+gl^- and Li^+gl^- conduction bands contain the frontier orbitals of Na^+ and Li^+ cations, and their valence bands comprise the frontier orbitals of O^{2-} and Cl^- in the glass electrolytes [20].

With respect to Li-MnO_2, Figure 4 shows the possibilities regarding the directions of the electron transfer based on ϕ^G_{CNL}. That is, as in the case of Na-Fc, there are two possibilities of intramolecular

electron transfer in adsorbed molecules $MnO_2Li^+_{(sf)}$(ad). One is from O^{2-}, responsible for the valence band of MnO_2, to $Li^+_{(sf)}$, responsible for the conduction band of Li^+gl^-. The other is from O^{2-} and Cl^-, which are responsible for the valence band of Li^+gl^-, to Mn(IV), responsible for the conduction band of MnO_2.

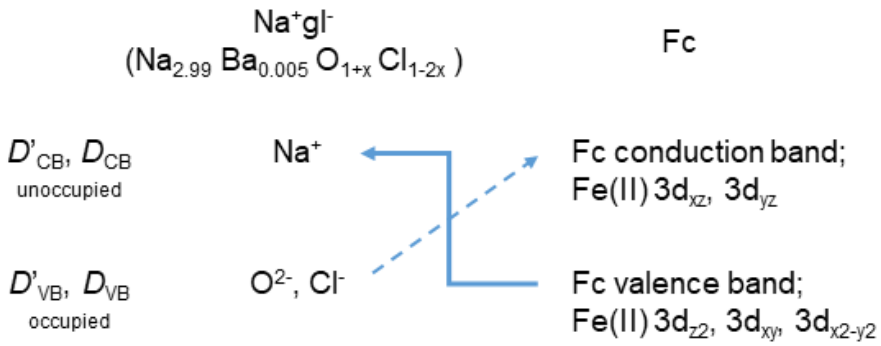

Figure 3. *Two possibilities of orbital hybridization in the theory of ϕ^G_{CNL} between Fc and Na^+gl^-. The inset arrows show the direction of possible electron transfer at their interfaces.* D'_{CB} *and* D'_{VB} *respectively correspond to the density of states of the conduction band and valence band of Na^+gl^-, and* D_{CB} *and* D_{VB} *respectively correspond to the density of states of the conduction band and valence band of Fc*

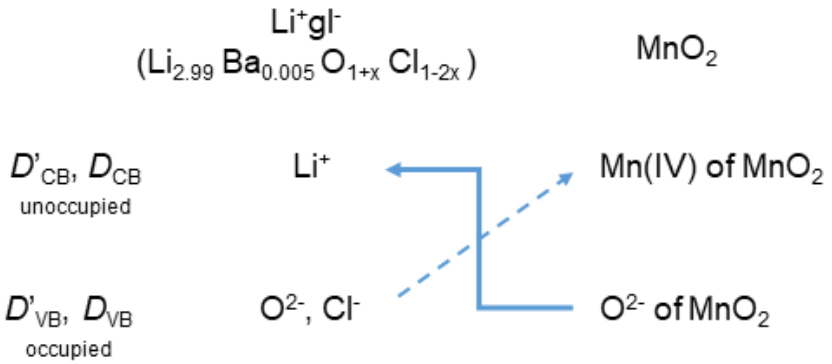

Figure 4. *Two possibilities of orbital hybridization in the theory of ϕ^G_{CNL} between MnO_2 and Li^+gl^-. The inset arrows show the direction of possible electron transfer at their interfaces.* D'_{CB} *and* D'_{VB} *respectively correspond to the density of states of the conduction band and valence band of Li^+gl^-, and* D_{CB} *and* D_{VB} *respectively correspond to the density of states of the conduction band and valence band of MnO_2*

In the former case, it is consistent with the experimental fact of Braga *et al*. [2] that Li is deposited. Therefore, the intramolecular electron transfer in adsorbed molecules of $MnO_2Li^+_{(sf)}$ (ad) and $MnO_2[2Li^+_{(sf)}$ (ad)] is in the direction from O^{2-} to $Li^+_{(sf)}$, as shown by the bold line in Figure 4.

From Figures 3 and 4, the deposition of Na and Li in the C[(CE)cC]*n* and C[2(CE)cC]*n* mechanisms is consistent with the results predicted in terms of ϕ^G_{CNL}. Therefore, in respect of intramolecular electron transfer appearing in both mechanisms, electron transfer occurs from Fc to $Na^+_{(sf)}$ and from MnO_2 to $Li^+_{(sf)}$, which are consistent with the ϕ^G_{CNL} views.

Na^+gl^- and Li^+gl^- are insulators [2]. Fc is a semiconductor [13], and MnO_2 is also a semiconductor [14] with a narrow band gap. In the case of Na-Fc and Li-MnO_2, the application of ϕ^G_{CNL} corresponds to the case of semiconductor-insulator interfaces. In this case, ϕ^G_{CNL} is given by Eq. (43):

$$\phi^G_{CNL} = E'_{VB} + E'_g|t_{VB'\text{-}CB}|^2 D_{CB}D'_{VB}/(|t_{VB'\text{-}CB}|^2 D_{CB}D'_{VB} + |t_{VB\text{-}CB'}|^2 D_{VB}D'_{CB}) \quad (43)$$

where E'_{VB}, E'_g, D'_{VB}, and D'_{CB} are the level of the valence band top, the band gap, the density of states of the valence bands, and the density of states of the conduction bands of Na^+gl^- or Li^+gl^-, respectively; D_{VB} and D_{CB} are the density of states of the valence bands and the density of states of the conduction bands of Fc or MnO_2, respectively; $|t_{VB'\text{-}CB}|$ is the transfer energy between valence band orbitals of

Na^+gl^- or Li^+gl^- and conduction band orbitals of Fc or MnO_2; $|t_{VB\text{-}CB'}|$ is the transfer energy between valence band orbitals of Fc or MnO_2 and conduction band orbitals of Na^+gl^- or Li^+gl^-. The terms of $|t_{VB'\text{-}CB}|^2 D_{CB} D'_{VB}$ and $|t_{VB\text{-}CB'}|^2 D_{VB} D'_{CB}$ correspond to effective bond strengths at the heterojunction interface [17]. Although Na^+gl^- and Li^+gl^- are amorphous structures, their band structures are expressed in terms of ordinary terminology because there is no obstacle in the ϕ^G_{CNL} analyses of these reaction mechanisms.

The theory ϕ^G_{CNL} is built on an orbital hybridization between the unoccupied and occupied states of two materials at an interface [15-19]. In this theory, the charge transfer between Fc and Na^+gl^- and MnO_2 and Li^+gl^- are realized by orbital hybridization between their unoccupied and occupied states. Their electron transfer is confined to just interfaces between Fc and Na^+gl^- and MnO_2 and Li^+gl^- because Na^+gl^- and Li^+gl^- demonstrate greater than 8eV band gap [2,4-6].

Eq. (43) is obtained by $\Delta\rho = 0$ in Eq. (44), which was derived by applying the second-order perturbation theory of quantum mechanics [17,24]. $\Delta\rho$ means transfer charges from Fc or MnO_2 to the insulator and proportional to the equation's right-hand side. At $\Delta\rho = 0$ in Eq. (44), the E_f corresponds to the Fermi level and the charge neutrality level for Fc after contacting $Na^+_{(sf)}$ and is identical to ϕ^G_{CNL} of Eq. (43). These relationships are the same for Li-MnO_2.

$$\Delta\rho \propto D_{VB} D'_{CB} |t_{VB\text{-}CB'}|^2 / (E'_{CB} - E_f) - D_{CB} D'_{VB} |t_{VB'\text{-}CB}|^2 / (E_f - E'_{VB}) \quad (44)$$

where E'_{CB} corresponds to the conduction band bottom of Na^+gl^- or Li^+gl^- in this study.

Assuming $D_{VB} = D_{CB}$ and $|t_{VB\text{-}CB'}|^2 = |t_{VB'\text{-}CB}|^2$ in (43), ϕ^G_{CNL} is consistent with the conventional charge neutrality level, ϕ_{CNL}, expressed in Eq. (45), and this ϕ_{CNL} is capable of demonstrating neither the effects of orbital hybridization nor those of the adsorption between Fc and $Na^+_{(sf)}$ and MnO_2 and $Li^+_{(sf)}$ [15-9,25].

$$\phi_{CNL} = E'_{VB} + E'_g D'_{VB} / (D'_{VB} + D'_{CB}) \quad (45)$$

In order to evaluate the effect of orbital hybridization, the magnitude of the second term on the right-hand side of Eq. (43) will be compared with Eq. (45) to evaluate the difference in electron energy levels at heterojunction interfaces with and without orbital hybridization.

In this study, let Eq. (43), which is ϕ^G_{CNL}, be transformed into Eq. (46) as follows:

$$\phi^G_{CNL} = E'_{VB} + E'_g D'_{VB} / (D'_{VB} + \Psi D'_{CB}) \quad (46)$$

where $\Psi = (|t_{VB\text{-}CB'}|^2 / |t_{VB'\text{-}CB}|^2)(D_{VB}/D_{CB})$.

In comparing Eq. (46) and Eq. (45), $\phi^G_{CNL} < \phi_{CNL}$ corresponds to $\Psi > 1$, and $\phi^G_{CNL} > \phi_{CNL}$ corresponds to $\Psi < 1$. Therefore, the relationship between ϕ_{CNL} and ϕ^G_{CNL} can be confirmed by examining Ψ. Therefore, depending on whether Ψ is greater than or less than 1, the difference in electron energy levels at heterojunction interfaces with and without orbital hybridization can be evaluated.

At first, $|t_{VB\text{-}CB'}|^2 / |t_{VB'\text{-}CB}|^2$ in Ψ is examined. From the results shown in Figure 3, in the case of Na-Fc, the electron transfer based on ϕ^G_{CNL} is from the valence band of Fc to the conduction of $Na^+_{(sf)}$. In the case of Li-MnO_2, Figure 4 shows that the electron transfer based on ϕ^G_{CNL} is from the valence band of MnO_2 to the conduction of $Li^+_{(sf)}$. Therefore, orbital hybridization is strong between these bands, so that, for both Na-Fc and Li-MnO_2, $|t_{VB\text{-}CB'}|^2 \gg |t_{VB'\text{-}CB}|^2$, *i.e.*, $|t_{VB\text{-}CB'}|^2 / |t_{VB'\text{-}CB}|^2 \gg 1$.

Next, consider (D_{VB}/D_{CB}) in Ψ. In the following (D_{VB}/D_{CB}) calculations, the density of states was represented by the number of states of orbitals in the energy levels actually relating to these battery reactions [26]. In the case of Fc in Na-Fc, the density of states for the valence band, D_{VB}, corresponds to the three orbitals $3d_{z2}$, $3d_{xy}$, and $3d_{x2\text{-}y2}$ of Fe(II) [13] located at the Fc center. The number of states in each orbital is 2, and thus the total is 2x3 = 6. On the other hand, the density of states for the conduction band, D_{CB}, corresponds to the two orbitals $3d_{xz}$ and $3d_{yz}$ of Fe(II) [13], which is 2x2 = 4.

Therefore, in the case of Fc, taking account of these $D_{VB} = 6$ and $D_{CB} = 4$, $(D_{VB}/D_{CB})_{Fc} > 1$. Therefore, $\Psi >> 1$ for the interface between $Na^+_{(sf)}$ and Fc, taking account of $|t_{VB\text{-}CB'}|^2/|t_{VB'\text{-}CB}| >> 1$ and $(D_{VB}/D_{CB})_{Fc} > 1$.

Therefore, in the case of Na-Fc, clearly $\Psi >> 1$, and clearly $\phi^G_{CNL} < \phi_{CNL}$. The electron energy level at the heterojunction interface with orbital hybridization is obviously lower than without orbital hybridization. Therefore, this finding indicates that when Fc and $Na^+_{(sf)}$ are in contact in the positive active materials, the formation of adsorbed molecules $FcNa^+_{(sf)}$(ad) and the associated intramolecular electron transfer due to orbital hybridization is more thermodynamically stable than when no orbital hybridization occurs.

Under Na-Fc open circuit conditions, at the Fc and $Na^+_{(sf)}$ heterojunction interface, intramolecular electron transfer forms a positive dipole on the Fc side, lowering the electron energy level of the Fc side and pushing up that of the $Na^+_{(sf)}$ side relatively, resulting in equilibrium at ϕ^G_{CNL} where the electron energy levels of both Fc and $Na^+_{(sf)}$ sides are balanced. This dipole state is retained under open circuit conditions.

Once a discharge state appears, the dipole at this heterojunction interface once disappears due to the electrochemical reaction of the E step following the interfacial intramolecular electron transfer C step in the (CE)c part of the C[(CE)cC]*n* mechanism. That is, as described in the former sections, under Na-Fc discharge conditions, the $Na^+_{(sf)}$ side is consequently reduced to Na by Fc side, Fc itself is oxidized to the Fc^+ intermediate, which is immediately reduced to Fc under the potential of the Na anode, and these reactions are repeated *n* times in the C[(CE)cC]*n* mechanism.

In the case of Li-MnO_2, two mechanisms were demonstrated as possibilities in the previous sections. One is the same C[(CE)cC]*n* mechanism as Na-Fc, and the other is the C[2(CE)cC]*n* mechanism. In respect of the term of $|t_{VB\text{-}CB'}|^2/|t_{VB'\text{-}CB}|^2$ in Ψ in Eq. (46), $|t_{VB\text{-}CB'}|^2/|t_{VB'\text{-}CB}|^2 >> 1$ for both Na-Fc and Li-MnO_2, as described above. Therefore, for Li-MnO_2, the term of $(D_{VB}/D_{CB})_{MnO_2}$ in Ψ in Eq.(46) has to be examined in order to confirm whether Ψ for Li-MnO_2 is greater than or less than 1.

At first, the C[(CE)cC]*n* mechanism for Li-MnO_2 is examined, where $Li^+_{(sf)}$ is adsorbed one-to-one against MnO_2, *i.e.*, the formation of adsorbed molecules $MnO_2Li^+_{(sf)}$(ad). As shown in Figure 4, in this case, D_{VB} corresponds to the 2p orbitals of $2O^{2-}$ per one $Li^+_{(sf)}$, so that the number of states of the 2p orbitals is $2\times(2\times3) = 12$. D_{CB} corresponds to the 3d orbitals of Mn(IV), which is $2\times5 = 10$. Thus, $(D_{VB}/D_{CB})_{MnO_2} > 1$ for the C[(CE)cC]*n* mechanism. Therefore, $\Psi >> 1$ for the heterojunction interface between $Li^+_{(sf)}$ and MnO_2 also results in $\phi^G_{CNL} < \phi_{CNL}$. In the C[(CE)cC]*n* mechanism, this result, $\phi^G_{CNL} < \phi_{CNL}$, indicates that when MnO_2 and $Li^+_{(sf)}$ are in contact with the positive active materials, the formation of adsorbed molecules $MnO_2Li^+_{(sf)}$(ad) and the associated intramolecular electron transfer due to orbital hybridization is also more thermodynamically stable than when no orbital hybridization occurs.

In the case of the C[2(CE)cC]*n* mechanism, the adsorption of two $Li^+_{(sf)}$ onto MnO_2 occurs simultaneously, *i.e.*, the formation of adsorbed molecules $MnO_2[2Li^+_{(sf)}(ad)]$. In this case, D_{VB} corresponds to the 2p orbitals of $2O^{2-}$ for two $Li^+_{(sf)}$, so that the number of states of the 2p orbitals per one $Li^+_{(sf)}$ is $1\times(2\times3) = 6$. On the other hand, D_{CB} corresponds to the 3d orbitals of Mn(IV), which is ten, as in the case of the C[(CE)cC]*n* mechanism. Therefore, $(D_{VB}/D_{CB})_{MnO_2} < 1$ for the C[2(CE)cC]*n* mechanism. Taking account of $|t_{VB\text{-}CB'}|^2/|t_{VB'\text{-}CB}|^2 >> 1$ and this $(D_{VB}/D_{CB})_{MnO_2} < 1$, it could be considered that $\Psi > 1$ for the interface between $2Li^+_{(sf)}$ and MnO_2, which also results in $\phi^G_{CNL} < \phi_{CNL}$. Consequently, the relationship between ϕ^G_{CNL} and ϕ_{CNL} for Li-MnO_2 is $\phi^G_{CNL} < \phi_{CNL}$ for both C[(CE)cC]*n* and C[2(CE)cC]*n* mechanisms.

As examined above, in the C[(CE)cC]*n* mechanism, $\phi^G_{CNL} < \phi_{CNL}$ is clear, but in the C[2(CE)cC]*n* mechanism, $\phi^G_{CNL} < \phi_{CNL}$ is not as clear as that for the C[(CE)cC]*n* mechanism. However, even for the C[2(CE)cC]*n* mechanism, this finding, $\phi^G_{CNL} < \phi_{CNL}$, is reasonable to assume that when MnO_2 and $2Li^+_{(sf)}$ are in contact in the positive active materials, the formation of adsorbed molecules MnO_2 $[2Li^+_{(sf)}(ad)]$ by orbital hybridization and the associated intramolecular electron transfer are thermodynamically stable than when no orbital hybridization occurs.

As in the case of Na-Fc, under Li-MnO_2 open circuit conditions, at the MnO_2 and $Li^+_{(sf)}$ heterojunction interface, intramolecular electron transfer forms a positive dipole on the MnO_2 side, lowering the electron energy level of the MnO_2 side and pushing up the energy level of the $Li^+_{(sf)}$ side relatively, resulting in equilibrium at ϕ^G_{CNL} where the electron energy levels of both MnO_2 and $Li^+_{(sf)}$ sides are balanced. This dipole state is retained under open circuit conditions.

Once a discharge state appears, as in the case of Na-Fc, the dipole at this heterojunction interface once disappears due to the electrochemical reaction of the E step following the interfacial intramolecular electron transfer C step in the (CE)c part of the C[(CE)cC]*n* mechanism and the 2(CE)c part of the C[2(CE)cC]*n* mechanism. That is, as described in the former sections, under Li-MnO_2 discharge conditions, the $Li^+_{(sf)}$ side is consequently reduced to Li by the MnO_2 side, MnO_2 itself is oxidized to the $Mn(O_2)^+$ intermediate, which is immediately reduced to MnO_2 under the potential of the Li anode, and these reactions are repeated *n* times in the mechanisms.

At the end of this section, we examine which mechanism, C[(CE)cC]*n* or C[2(CE)cC]*n*, is more thermodynamically favorable for Li-MnO_2. As shown above, $(D_{VB}/D_{CB})_{MnO_2} < 1$ in the C[2(CE)cC]*n* mechanism. On the contrary, $(D_{VB}/D_{CB})_{MnO_2} > 1$ in the C[(CE)cC]*n* mechanism. The value of $|t_{VB\text{-}CB'}|^2/|t_{VB'\text{-}CB}|^2$ is common as $|t_{VB\text{-}CB'}|^2/|t_{VB'\text{-}CB}|^2 >> 1$ in both mechanisms. Therefore, Ψ for C[(CE)cC]*n* is obviously bigger than that for C[2(CE)cC]*n*, which means that ϕ^G_{CNL} for C[(CE)cC]*n* is lower than that for C[2(CE)cC]*n* from Eq. (46). Therefore, the C[(CE)cC]*n* mechanism for Li-MnO_2 is considered to be more thermodynamically stable than the C[2(CE)cC]*n* mechanism.

The C[2(CE)cC]*n* mechanism requires two $Li^+_{(sf)}$ to form adsorption orbitals simultaneously, which seems to be less probable than the C[(CE)cC]*n* mechanism. This intuitive view is compatible with the results of the ϕ^G_{CNL} analysis. Taking these findings into consideration, although ϕ^G_{CNL} indicates that the C[2(CE)cC]*n* mechanism is still possible, the C[(CE)cC]*n* mechanism is considered to be dominant in the Li-MnO_2 cathode reactions.

Limitations of the alkali metal deposition cycle

In mechanism-based stoichiometry, the maximum number of cycles of alkali metal deposition at the positive electrodes per mole of Fc and MnO_2 is $n = p$ for C[(CE)cC]*n* and $n = p/2$ for C[2(CE)cC]*n*, as described in the previous section. With regard to this *p*-value, this specific value per actual effective mole of Fc and MnO_2 will be considered in this section.

In order to do this, $(M_{Fc})_{eff}$ and $(M_{MnO_2})_{eff}$ are introduced, where $(M_{Fc})_{eff}$ and $(M_{MnO_2})_{eff}$ are the effective molalities (mol/kg) of Fc and MnO_2 in the positive active materials, respectively. In general, the activity of a reactive species does not numerically match its concentration determined in the reagent preparation stage. Since the utilization coefficient is used as a parameter for active material utilization in practical batteries, in the same way, the utilization coefficient λ is introduced here. In practice, $\lambda_{Fc} = (M_{Fc})_{eff}/(M_{Fc})_{mes}$ for Na-Fc, and $\lambda_{MnO_2} = (M_{MnO_2})_{eff}/(M_{MnO_2})_{mes}$ for Li-MnO_2, where $(M_{Fc})_{mes}$ and $(M_{MnO_2})_{mes}$ are defined as the molalities of Fc and MnO_2 determined at the preparation stage of the positive active materials, respectively. Taking account of λ_{Fc} and λ_{MnO_2}, $(M_{Fc})_{eff} = \lambda_{Fc}(M_{Fc})_{mes}$ and $(M_{MnO_2})_{eff} = \lambda_{MnO_2}$ $(M_{MnO_2})_{mes}$. Therefore, to determine the actual maximum number of cycles of the

alkali metal deposition at the positive electrodes, not only the specific *p*-value but also λ_{Fc} for $(M_{Fc})_{eff}$ and λ_{MnO_2} for $(M_{MnO_2})_{eff}$ have to be determined.

First, the procedure to determine the specific *p*-value is examined, assuming that both $(M_{Fc})_{eff}$ and $(M_{MnO_2})_{eff}$ are fixed at 1 mol/kg. That is, the specific *p*-value, *i.e.* the maximum number of cycles of alkali metal deposition, demonstrated in this section corresponds to the case for $(M_{Fc})_{eff} = (M_{MnO2})_{eff} =$ = 1 mol/kg. The determination procedures of λ_{Fc} for $(M_{Fc})_{eff}$ and λ_{MnO_2} for $(M_{MnO_2})_{eff}$ will be examined in detail in the next section, and the maximum discharge capacity of Na-Fc and Li-MnO_2 positive electrodes will be examined, taking account of the *p*-values corresponding to $(M_{Fc})_{eff} = (M_{MnO2})_{eff}$ = 1 mol/kg determined in this section. In the case of Li-MnO_2, ϕ^G_{CNL} studies indicate that the C[(CE)cC]*n* mechanism is more thermodynamically favorable than the C[2(CE)cC]*n* mechanism, and the discharge results are the same for both Li-MnO_2 mechanisms. Therefore, in the following, the C[(CE)cC]*n* mechanism will be used to describe the reaction mechanism for Na-Fc and Li-MnO_2.

The number of $Na^+_{(sf)}$ and $Li^+_{(sf)}$ available for adsorption onto Fc and MnO_2 in the positive active materials, *i.e.* those in contact at x_0 position in Figure 2, is the *p*-value itself appearing in the C[(CE)cC]*n* mechanism. As discussed in the previous section, the closest distance of $Na^+_{(sf)}$ and $Li^+_{(sf)}$ to Fc and MnO_2 was considered to be *ca.* 200pm. Therefore, it is necessary to examine the *p*-value at this x_0 position. In this section, this *p*-value will be evaluated by steps 1-5 as follows:

1. From the size of the unit crystal lattice of Fc and MnO_2, consider a new size lattice with axes that are stretched by 200 pm each to the left, right, top, and bottom of each axis of each unit crystal lattice for a total of 400 pm larger for each axis.
2. Find the total surface area of the new lattice size. Find how many times this total surface area corresponds to the area of the circle, taking into account of radii, *r*, of $Na^+_{(sf)}$ and $Li^+_{(sf)}$, respectively, expressed as (total surface area)/πr^2, for Fc as (S_{Fc}/S_{Na+}) and for MnO_2 as (S_{MnO_2}/S_{Li+}).
3. Find the number of Fc and Mn involved in the unit crystal lattice and denote it as N_{Fc} and N_{Mn}, respectively.
4. Introduce a factor of f_S for the area factor, which is the fraction of the total surface area of this large new lattice that is actually occupied by $Na^+_{(sf)}$ and $Li^+_{(sf)}$ because the surface of the new lattice of Fc and MnO_2 will be in common contact with the glass solid electrolyte as well as carbon black.
5. Introduce a factor f_P relating to the porosity of the positive active materials, where f_P = 1- (porosity of positive active materials)/100.

From 1-5 above, the maximum *p*-value per effective molality of 1 mol/kg of Fc, $(p_{Fc})_{max}$, and that per effective molality of 1 mol/kg of MnO_2, $(p_{MnO_2})_{max}$, are given by the following Eqs. (47) and (48), respectively.

$$(p_{Fc})_{max} = f_S f_P (S_{Fc}/S_{Na+})/N_{Fc} \quad (47)$$

$$(p_{MnO_2})_{max} = f_S f_P (S_{MnO_2}/S_{Li+})/N_{Mn} \quad (48)$$

Figure 5 shows a schematic of $Na^+_{(sf)}$ around the Fc unit crystal lattice and Na deposited on discharge. The projected plane of the solid line is the *bc* plane of the unit crystal lattice of Fc. The Fc crystal is the monoclinic system, with crystal axes *a* = 1050, *b* = 763, *c* = 595 pm and axis angles $\alpha = \gamma = 90°$ and $\beta = 121°$. The β angle corresponds to the angle between the *a* and *c* axes. The Fc number involved in the unit crystal lattice is N_{Fc} = 2. This data can be referred to elsewhere. The dashed line corresponds to the solid line extended 200 pm to the left and right of the *b* axis and 200 pm above and below the *c* axis. $Na^+_{(sf)}$ and Na tangent to the dashed line are on the *ab* and *ac* planes. Other $Na^+_{(sf)}$ and Na are projected onto the *bc* plane.

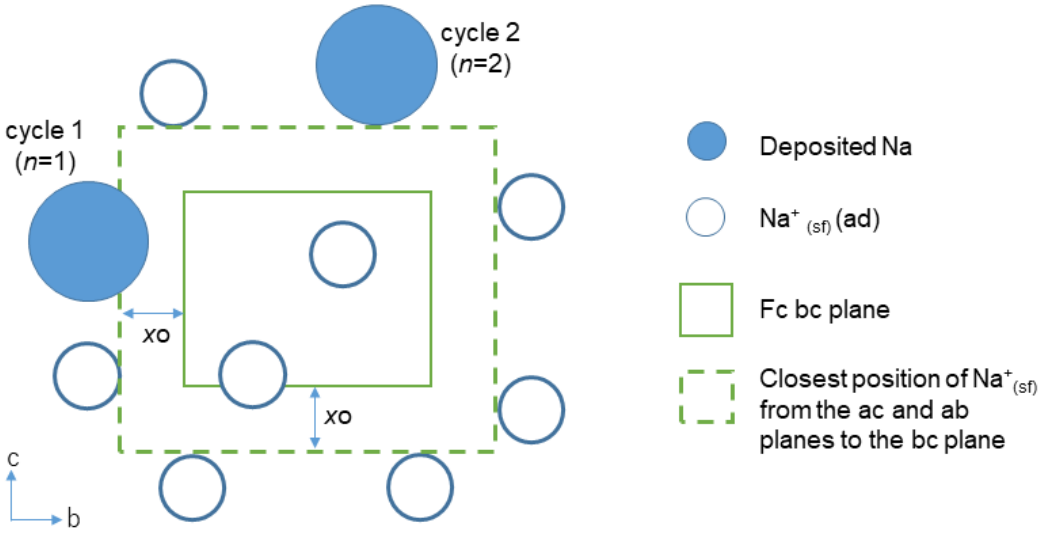

Figure 5. *An image of Fc monoclinic bc plane projection and $Na^+_{(sf)}$ and deposited Na. Circles and dark ones correspond to adsorbable $Na^+_{(sf)}$ and Na deposited in each discharge cycle. Circle radii reflect those of 186 Na and 99 Na^+ in comparison with the Fc monoclinic system axes of* b *= 763 and* c *= 595 pm for the unit cell.* x_0 *is 200 pm, which is the closest distance of $Na^+_{(sf)}$ to the unit cell*

In Figure 5, $Na^+_{(sf)}$ and Na total 10. Thus, in this case, the *p*-value in Eq. (1) is at most 10. Two of these are shown depositing as Na on discharge. The first cycle shows Na deposition corresponding to cycle number n = 1 and the second cycle to n = 2. Here, 8 $Na^+_{(sf)}$ are left, therefore when all of these are discharged, the number of cycles of Na deposition will reach a maximum at 10.

Although there is no specific information on the amounts of Fc, MnO_2, carbon black, Na^+gl^- powder, and Li^+gl^- powder in the preparation of the positive active materials [2], realistic estimates for f_S and f_P for the evaluation of $(p_{Fc})_{max}$ are to be employed. Based on the above step 2, (S_{Fc}/S_{Na+}) is directly calculated as $[2\times(1450\times1163)+2\times(1163x995)+2\times(1163\times1450\sin59°)]/99^2\pi$ = 277.6. The radius of $Na^+_{(sf)}$ is replaced with 99 pm of Na^+. Radius data on Na^+ can be referred to elsewhere. Assuming that f_S for $Na^+_{(sf)}$ is 0.5 and f_P is 0.5, $(p_{Fc})_{max}$ is 0.5×0.5×277.6/2 = 34.7 from Eq. (47) with N_{Fc} as 2. These values of f_S = 0.5 and f_P = 0.5 are considered realistic range values. Rounding down to the decimal point, $(p_{Fc})_{max}$ = 34. Therefore, in the case of Na-Fc, under the above conditions, the maximum number of reaction cycles n corresponding to n moles of Na deposition in the C[(CE)cC]n mechanism is 34 per effective molality of 1 mol/kg of Fc.

Figure 6 shows a projection schematic of $Li^+_{(sf)}$ around the β-MnO_2 unit crystal lattice and Li deposited by partial discharge reactions. The crystal structure of β-MnO_2 is the tetragonal system with crystal axes a = 440, b = 440, and c = 290 pm, the most compact and simplest of all MnO_2 crystal structures. The number of MnO_2 in the unit crystal lattice is N_{Mn} = 2. These data can be referred to elsewhere. The projection plane is the ab plane, and the shape of the solid line is similar to the ab plane of the unit crystal lattice of β-MnO_2. The dashed line corresponds to the solid line extended 200 pm above and below the a-axis and 200 pm to the left and right of the b-axis. $Li^+_{(sf)}$ and Li tangent to the dashed line are on the ac and bc planes. The other $Li^+_{(sf)}$ and Li are imaged as projected on the ab plane. In Figure 6, $Li^+_{(sf)}$ and Li total 10.

Therefore, in this case, the *p*-value in Eq. (1) is at most 10. Two of these are Li deposited in the discharge reaction. In Figure 6, cycle 1 shows Li deposition corresponding to cycle number n = 1 and cycle 2 to n = 2. Since 8 $Li^+_{(sf)}$ are left, if these are all discharged, the number of Li deposition cycles will be a maximum at 10.

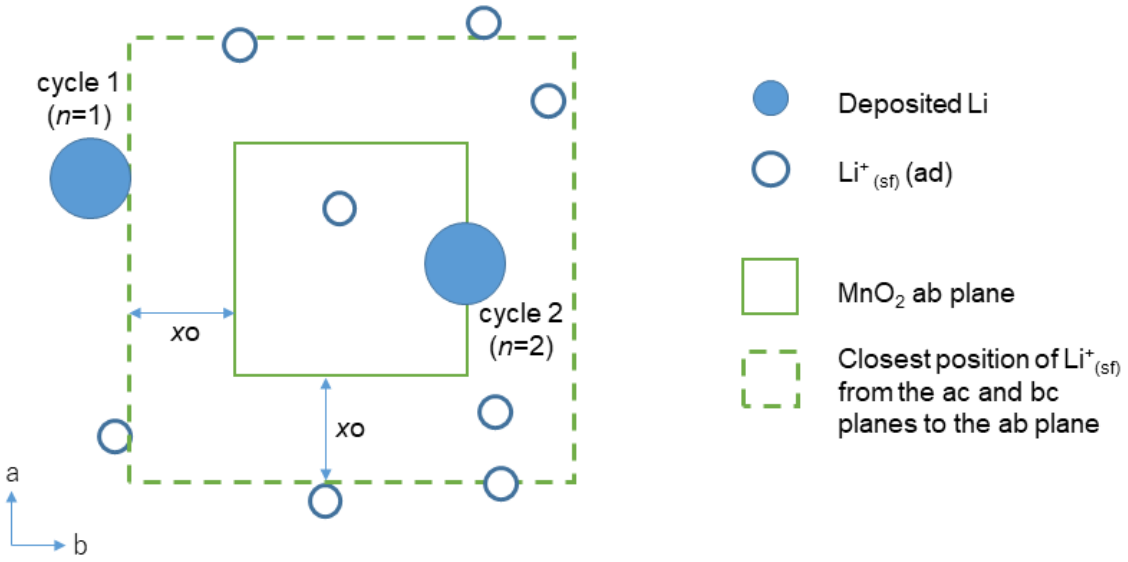

Figure 6. *An image of β-MnO_2 tetragonal ab plane projection and $Li^+_{(sf)}$ and deposited Li. Circles and dark ones correspond to adsorbable $Li^+_{(sf)}$ and Li deposited in each discharge cycle. Circle radii reflect those of 152 Li and 59 Li^+ in comparison with the β-MnO_2 tetragonal system axes of* a *= 440 and* b *= 440 pm for the unit cell.* x_0 *is 200 pm, which is the closest distance of $Li^+_{(sf)}$ to the unit cell*

In examining $(p_{MnO_2})_{max}$ using Eq. (48), as in the case of Na-Fc, estimates for f_S and f_P are used. Based on the above step 2, (S_{MnO_2}/S_{Li+}) is directly calculated as $[2\times8402+4\times(840\times690)]/59^2\pi = 342$. The radius of $Li^+_{(sf)}$ is replaced with 59 pm of Li^+. Radius data on Li^+ can be referred to elsewhere. Assuming that f_S for $Li^+_{(sf)}$ is 0.5 and f_P is 0.5, $(p_{MnO_2})_{max} = 0.5x0.5x342/2 = 42.8$ from Eq. (48) with N_{Mn} as 2. As described above, $f_S = 0.5$ and $f_P = 0.5$ are considered realistic range values. Therefore, in the case of Li-MnO_2, under the above conditions, the maximum number of reaction cycles *n* corresponding to *n* moles of Li deposition in the C[(CE)cC]*n* mechanism is 42 per effective molality of 1 mol/kg of MnO_2 when the decimal point of $(p_{MnO_2})_{max} = 42.8$ is rounded down to 42.

In the above discussions, f_S and f_P are factors that obviously depend on the conditions for the preparation of the positive active materials. Therefore, $(p_{Fc})_{max}$ and $(p_{MnO_2})_{max}$ are sensitive to f_S and f_P. When a 0.1 increase in f_S from 0.5 to 0.6 results in $(p_{Fc})_{max} = 41.6$ from 34.7 and $(p_{MnO_2})_{max} = 51.3$ from 42.8, care should be taken in discussing the first digit of the above values of the factors.

MnO_2 has several types of crystal systems. In the systems, both β-MnO_2 and γ-MnO_2 are used in batteries, and γ-MnO_2 has long been known to have better battery properties [27]. It was not clear in the paper [2] which type of MnO_2 was used, but γ-MnO_2 [28] seems to have been employed. β-MnO_2 contains two MnO_2 in the unit crystal lattice and has the highest electrical conductivity of all MnO_2 crystal systems due to the shortest Mn-Mn distance and small band gap [14]. γ -MnO_2 is a large lattice size containing four MnO_2, and its crystal structure is more complex than that of β-MnO_2. The unit crystal lattice size of β-MnO_2 is the smallest among the various MnO_2 crystal systems, and the crystal lattice surface area of β-MnO_2 per Mn is smaller than that of γ-MnO_2 per Mn [27], which $(S_{MnO_2}/S_{Li+})/N_{Mn}$ is smaller for β-MnO_2 than for γ-MnO_2. Therefore, the maximum number of cycles $(p_{MnO_2})_{max}$ is smaller for β-MnO_2 than for γ-MnO_2.

Braga *et al.* use the expression "self-charging," [5,6,28], which in the C[(CE)cC]*n* mechanism would correspond to an increase in the *p*-value. An increase in the *p*-value leads to an increase in discharge capacity. As described in the C[(CE)cC]*n* mechanism, under charge-discharge cycle conditions, it is naturally considered that the *p*-value appearing in Eq. (1) changes from cycle to cycle

as the charge-discharge cycle progress. It is considered that an increase in the effective density of $Na^+_{(sf)}$ for Na-Fc and $Li^+_{(sf)}$ for Li-MnO_2 after charging corresponds to being capable of increasing the *p*-value.

Discharge capacity

In this section, the pragmatic maximum discharge capacity of Na-Fc and Li-MnO_2 cathodes will be examined on the basis of $(p_{Fc})_{max}$ in Eq. (47) and $(p_{MnO_2})_{max}$ in Eq. (48). In order to do this, it is necessary to determine the utilization coefficients λ_{Fc} and λ_{MnO_2} to determine $(M_{Fc})_{eff}$ and $(M_{MnO_2})_{eff}$, as described in the previous section. Taking account of λ_{FC}, λ_{MnO_2}, $(p_{Fc})_{max}$, and $(p_{MnO_2})_{max}$, the actual maximum discharge capacity of Na-Fc and Li-MnO_2 cathodes are directly obtained from the following Eqs. (49) and (50), respectively.

$$(Q_{max})_{(Na\text{-}Fc)} = (\lambda_{Fc})[(M_{Fc})_{mes}][(p_{Fc})_{max}]F \text{ (C)} \quad (49)$$

$$(Q_{max})_{(Li\text{-}MnO_2)} = (\lambda_{MnO_2})[(M_{MnO_2})_{mes}][(p_{MnO_2})_{max}]F \text{ (C)} \quad (50)$$

where $(Q_{max})_{(Na\text{-}Fc)}$ and $(Q_{max})_{(Li\text{-}MnO_2)}$ represent the pragmatic maximum discharge capacity of Na-Fc and Li-MnO_2 positive electrodes, respectively; $(\lambda_{Fc})[(M_{Fc})_{mes}] = (M_{Fc})_{eff}$ and $(\lambda_{MnO_2})[(M_{MnO_2})_{mes}] = (M_{MnO_2})_{eff}$.

It is apparent that even though 1 mol/kg of Fc and MnO_2 is prepared at the preparation stage of the positive active materials, 1 mol/kg of Fc and MnO_2 is not dispersed as a single unit crystal lattice in the positive active materials, but they are present in a state of clusters. Therefore, the unit crystal lattice of Fc and MnO_2 inside clusters cannot participate in the adsorption equilibrium reactions. Therefore, obviously, $\lambda_{Fc} < 1$ and $\lambda_{MnO_2} < 1$ as in the case of ordinary batteries.

In order to estimate these practical values for λ_{Fc} and λ_{MnO_2}, simple cubic and rectangular blocks were considered. That is, each of these blocks was assumed as a unit crystal lattice, and the outer surface area of a block formed in one piece by several blocks was compared to the sum of the surface areas of each unit block. In this case, λ can be expressed as λ = (outer surface area of block assembly)/(sum of surface areas of each individual unit block), which can be basically equivalent to $(M_{Fc})_{eff}/(M_{Fc})_{mes}$ and $(M_{MnO_2})_{eff}/(M_{MnO_2})_{mes}$ as defined in the previous section.

The results showed that the rate of decrease in λ with respect to the rate of increase in the number of unit blocks is the largest when these unit blocks are connected by the same number of unit blocks on the *xyz* axis and assembled into a shape similar to that of the unit block. On the other hand, if the blocks are connected in only one of the *xyz* axis, the rate of decrease in λ is the smallest relative to the rate of increase in the number of unit blocks.

In the former case, λ can be simplified to $\lambda = 1/q$ for the homomorphism unified by *q* cubes or *q* rectangles where *q* is the number of cubic or rectangular unit blocks: *e.g.* for $q = 2$, $\lambda = 0.5$; for $q = 5$, $\lambda = 0.2$; for $q = 10$, $\lambda = 0.1$. In the latter case, the relationship between λ and the number of blocks is not simple: $\lambda = 0.83$ for a sequence of 2, $\lambda = 0.73$ for a sequence of 5, and $\lambda = 0.70$ for a sequence of 10, with an asymptote around 0.67.

In practice, λ is considered to be present between these two extreme conditions. When $\lambda = 0.1$ from the former case and $\lambda = 0.73$ from the latter case are taken into account, a pragmatic value of λ is considered to be around in the middle of the range between $\lambda = 0.73$ and 0.1, which seems to be around $\lambda = 0.4$.

When $\lambda_{Fc} = \lambda_{MnO_2} = 0.4$ and $(M_{Fc})_{mes} = (M_{MnO_2})_{mes} = 1$ mol/kg, $(\lambda_{Fc})(M_{Fc})_{mes} = (\lambda_{MnO_2})(M_{MnO_2})_{mes} = 0.4$ mol/kg for $(M_{Fc})_{eff}$ and $(M_{MnO_2})_{eff}$. In these cases, from Eqs. (49) and (50), the maximum discharge capacity of the Na-Fc positive electrode is $(0.4\times34)F = 13.6F$ (C), and that of the Li-MnO_2 positive electrode is $(0.4\times42)F = 16.8F$ (C). Under the above conditions, the discharge capacity of

the Na-Fc positive electrode is about 14*F* (C), which corresponds to 14 cycles of Na deposition corresponding to 14 moles of Na. In the case of Li-MnO_2, the discharge capacity of the positive electrode is about 17*F* (C), which corresponds to 17 cycles of Li deposition corresponding to 17 moles of Li.

In respect of the positive active materials for Na-Fc and Li-MnO_2, in accordance with the C[(CE)cC]*n* and C[2(CE)cC]*n* mechanisms and Eqs. (47) to (50), both Fc and Na^+gl^- correspond to those for Na-Fc, and both MnO_2 and Li^+gl^- correspond to those for Li-MnO_2. As shown in Eqs. (49) and (50), $(Q_{max})_{(Na\text{-}Fc)}$ and $(Q_{max})_{(Li\text{-}MnO_2)}$ are proportional to the amount of Fc and MnO_2 in terms of $(\lambda_{Fc})[(M_{Fc})_{mes}]$ and $(\lambda_{MnO_2})[(M_{MnO_2})_{mes}]$, respectively. That is, Fc and MnO_2 obviously play the role of active materials. Fc and MnO_2, on the other hand, act as catalysts, as indicated in the previous sections. Therefore, preparing the amount of Fc and MnO_2 is considered equivalent to preparing the amount of catalyst.

Na^+gl^- and Li^+gl^- affect $(p_{Fc})_{max}$ in Eq. (47) and $(p_{MnO_2})_{max}$ in Eq. (48), respectively, and each of $(p_{Fc})_{max}$ and $(p_{MnO_2})_{max}$ consists of mainly three parameters. On the other hand, with regard to Fc and MnO_2, the relationships between $(M_{Fc})_{mes}$ and $(M_{Fc})_{eff}$ and $(M_{MnO_2})_{mes}$ and $(M_{MnO_2})_{eff}$ are simple as controlling parameters of the discharge capacity because these pairs of parameters are connected in terms of only one parameter of λ. Therefore, it is considered that Fc and MnO_2 are simpler and more straightforward than Na^+gl^- and Li^+gl^- as controlling parameters for the positive electrode capacity. Taking account of these findings, it seems simple and appropriate to consider the capacity of the positive electrode represented by $(M_{Fc})_{mes}$ and λ_{Fc} for Na-Fc and $(M_{MnO_2})_{mes}$ and λ_{MnO_2} for MnO_2.

As with conventional batteries, if the capacity of Na and Li negative electrodes is sufficient above that of the positive active materials, the discharge capacity of Na-Fc and Li-MnO_2 will be determined by each capacity of the positive electrodes, and vice versa. However, the capacity balance between the cathodes and anodes of Na-Fc and Li-MnO_2 is considered very specific in this respect, as is the Braga-Goodenough Li-S [2,8]. In order to balance the discharge capacity between the anode and cathode, when $\lambda_{Fc} = \lambda_{MnO_2} = 0.4$ and $(M_{Fc})_{mes} = (M_{MnO_2})_{mes} = 1$ mol/kg, the capacity of the Na anode of Na-Fc is required to be at least 14 times higher than that of the cathode, and the capacity of the Li anode of Li-MnO_2 is required to be at least 17 times higher than that of the cathode. That is, for Fc and MnO_2 with an effective molality of 0.4 mol/kg, the Na anode capacity of Na-Fc and the Li anode capacity of Li-MnO_2 need an effective molality equivalent to at least 14 and 17 times the capacity of the cathode, respectively. According to Braga *et al*. [2], the discharge capacity of Na-Fc and Li-MnO_2 was controlled by the Na and Li anodes. Although this fact [2] is simply considered to be ascribed to a lack of the capacity of alkali metal anodes, taking account of the capacity balance between the anodes and cathodes of Na-Fc and Li-MnO_2 in terms of the mechanisms as described in this paper, the battery capacity determination of Na-Fc and Li-MnO_2 by the alkali metal anodes is considered to be plausible and comprehensible.

Based on the above findings, Na-Fc and Li-MnO_2, including Braga-Goodenough Li-S, appear to be absolutely different from the conventional concept of cathode capacity limits for alkali metal anodes.

Optimization of the positive active materials of the Braga-Goodenough rechargeable batteries was not performed [2]. If it had been done, the performance of these batteries would have been much enhanced. Orthogonal array experiments are necessary to obtain the actual maximum capacity of the cathodes because multiple factors are involved with respect to active materials, as shown in Eqs. (47)-(50). Possible control factors other than Eqs. (47)-(50) in orthogonal array experiments may include the reagent manufacturer, the powder mesh number, the pressure on the active materials, and so on.

Conclusions

Concerning the cathode deposition of alkali metals during discharge in Na-Fc and Li-MnO_2, two new types of the C[(CE)cC]*n* and C[2(CE)cC]*n* mechanisms were proposed. These reaction mechanisms were obtained by the results of complementary analyses between the chemical and electrochemical viewpoints and the solid-state physics and heterojunction physics, ϕ^G_{CNL}, viewpoints on the solid/solid contact interfaces. ϕ^G_{CNL}, the theory of generalized charge neutrality level, has provided critical decision criteria for examining these reaction mechanisms with regard to orbital hybridization and intramolecular electron transfer, which are directly related to the adsorption and alkali metal deposition in these mechanisms.

The Na-Fc mechanism corresponds to a multi-step C[(CE)cC]*n* mechanism where C is the chemical reaction, E is the electrochemical reaction, c is the catalytic (CE) step, and *n* is the *n*-cycle of the [(CE)cC] step. The nth cycle corresponds to *n* moles of Na or Li deposition. In the case of Li-MnO_2, two mechanisms were considered. One is the C[(CE)cC]*n* mechanism, which is the same as Na-Fc, and the other is the C[2(CE)cC]*n* mechanism, in which the (CE) of the catalytic reaction 2(CE)c is two consecutive steps. In the C[(CE)cC]*n* mechanism, $Na^+_{(sf)}$ and $Li^+_{(sf)}$ form one-to-one adsorption onto Fc and MnO_2, respectively. On the other hand, in the C[2(CE)cC]*n* mechanism of Li-MnO_2, two $Li^+_{(sf)}$ absorb simultaneously onto MnO_2. Although the elementary reactions in the two mechanisms of Li-MnO_2 were different, the same results were obtained for the discharge capacity and deposited Li content. In the two mechanisms of Li-MnO_2, ϕ^G_{CNL} analysis indicated that the C[(CE)cC]*n* mechanism lowered the charge neutrality level more than the C[2(CE)cC]*n* mechanism, indicating that the C[(CE)cC]*n* mechanism is dominant and more thermodynamically stable than the C[2(CE)cC]*n* mechanism. In this regard, the C[(CE)cC]*n* mechanism is considered to be representative of these cathode reactions.

In both mechanisms, the first C and the third C are the steps in the formation of adsorption equilibrium. In the second C step corresponding to the C in the (CE) part, Fc and MnO_2 reduce $Na^+_{(sf)}$ and $Li^+_{(sf)}$ to deposit Na and Li, respectively, which correspond to intramolecular charge transfer reactions within adsorbed molecules during discharge. Fc and MnO_2 are themselves oxidized to Fc^+ and $Mn(O_2)^+$ intermediates, respectively, which are immediately reduced to Fc and MnO_2 under alkali metal anode potentials in the subsequent E step. Fc and MnO_2 act as catalysts in these (CE)c and 2(CE)c steps because they are not consequently changed on discharge.

In the case of Na-Fc, the orbital hybridization involving adsorption occurs between the conduction band orbital of $Na^+_{(sf)}$ and the valence band orbital of Fc. In the case of Li-MnO_2, this orbital hybridization occurs between the conduction band orbital of $Li^+_{(sf)}$ and the valence band orbital of $2O^{2-}$ in MnO_2. The direction of intramolecular electron transfer is from the valence band orbital of Fc to the conduction band orbital of $Na^+_{(sf)}$ for Na-Fc and from the valence band orbital of $2O^{2-}$ in MnO_2 to the conduction band orbital of $Li^+_{(sf)}$ for Li-MnO_2.

The maximum alkali metal deposition and maximum discharge capacity of Na-Fc and Li-MnO_2 cathodes were evaluated on the basis of these mechanisms and found to be essentially determined by the effective number of $Na^+_{(sf)}$ and $Li^+_{(sf)}$ contacts that can hybridize orbitals with Fc and MnO_2 and the effective molality of Fc and MnO_2 in the positive active materials. Algorithms for determining the effective contact numbers of $Na^+_{(sf)}$ and $Li^+_{(sf)}$ and the effective molality of Fc and MnO_2 were examined. To determine the effective contact numbers of $Na^+_{(sf)}$ and $Li^+_{(sf)}$, it was necessary to determine the closest distance of these ions to the Fc and MnO_2 unit crystal lattices and introduce parameters such as the area fraction of these ions in relation to the total surface area around the Fc and MnO_2 unit crystal lattices at the closest distance being 200 pm. To determine the

effective molality of Fc and MnO_2, it was necessary to introduce their utilization coefficients in the positive active materials.

As a result employing realistic values of these parameters, when the effective molality of Fc and MnO_2 was 0.4 mol/kg, the number of alkali metal deposition cycles of the cathodes in the C[(CE)cC]*n* mechanism was about 14 for Na-Fc and about 17 for Li-MnO_2, and the deposition of alkali metals amounted to about 14 moles Na for Na-Fc and about 17 moles Li for Li-MnO_2, and cathode discharge capacities corresponding to these were about 14*F* (C) for Na-Fc and about 17*F* (C) for Li-MnO_2. In this respect, the anode capacities of Na and Li to balance these cathode capacities were more than 14*F* (C) for the Na anode capacity of Na-Fc and more 17*F* (C) for the Li anode capacity of Li-MnO_2. Therefore, for Fc and MnO_2 with an effective molality of 0.4 mol/kg, the Na anode of Na-Fc and the Li anode of Li-MnO_2 needed to have an effective molality equivalent to at least 14 and 17 times the capacity of the cathode, respectively.

On the basis of these C[(CE)cC]*n* and C[2(CE)cC]*n* mechanisms, the self-charging phenomenon described by Braga *et al.* [5,6,28] was considered to be attributed to an increase in the effective number of $Na^+_{(sf)}$ and $Li^+_{(sf)}$ contacts that can hybridize orbitals with Fc and MnO_2 during charge-discharge cycling.

Conflict of interest: *This paper is free of conflict of interest.*

Acknowledgements: *The author thanks Takahiro Hidaka for helpful discussions on ligand field chemistry.*

Appendix

Charge neutrality level in heterojunction

The concept of charge neutrality level appeared more than half a century ago [29,30], but was only observed experimentally in 2000 [31,32]. The charge neutrality level can be regarded as the effective E_f on the semiconductor and insulator side relative to the Schottky barrier, and charge transfer takes place to match the E_f of the metal with the charge neutrality level of the semiconductor and insulator at the interface [17].

The theory of generalized charge neutrality level, ϕ^G_{CNL}, emerged around 2005 [15-19]. ϕ^G_{CNL} in a heterojunction is characterized by the energy and density of states of the bands of the materials on both sides and by orbital hybridization at their contact interfaces [15-19]. On the other hand, the conventional ϕ_{CNL} consists of the energy and density of states of the bands for a one-sided material [25]. ϕ_{CNL} cannot handle orbital hybridization at the contact interface and the associated charge transfer. In recent years, problems such as tunneling leakage currents have arisen due to the increasing integration of electronic devices into nano-devices, and high-*k* insulators have attracted attention as a material for solving these problems. HfO_2, a candidate for the high-*k* insulators, exhibited behavior that was difficult to resolve with conventional understanding of heterojunction interfaces, and this ϕ^G_{CNL} succeeded in clarifying this Schottky barrier behavior [15-19]. ϕ^G_{CNL} can be extended from the Schottky barrier in metals/insulators to the evaluation of semiconductor/insulator and semiconductor/semiconductor band discontinuities [15-19].

References

[1] K. Waki, *Sulfur/Carbon Composite Electrodes for Lithium-Sulfur Batteries,* Strategy for Technology Development, Proposal paper for Policy Making and Governmental Action

toward Low Carbon Societies, Center for Low Carbon Society Strategy, Japan Science and Technology Agency, February (2018). https://www.jst.go.jp/lcs/en

[2] M. H. Braga, N. S. Grundish, A. J. Murchison, J. B. Goodenough, *Energy and Environmental Science* **10** (2017) 331-336. https://dx.doi.org/10.1039/c6ee02888h

[3] D. A. Streingart, V. Viswanathan, *Energy and Environmental Science* **11** (2018) 221-222. https://dx.doi.org/10.1039/c7ee01318c

[4] M. H. Braga, A. J. Murchison, J. A. Ferreira, P. Singh, J. B. Goodenough, *Energy and Environmental Science* **9** (2016) 948-954. https://doi.org/10.1039/C5EE02924D

[5] M. H. Braga, C. M. Subramaniyam, A. J. Murchison, J. B. Goodenough, *Journal of the American Chemical Society* **140** (2018) 6343. https://dx.doi.org/10.1021/jacs.8b02322

[6] M. H. Braga, J. E. Oliveira, A. J. Murchison, J. B. Goodenough, *Applied Physics Reviews* **7** (2020) 011406. https://dx.doi.org/10.1063/1.5132841

[7] *University of Texas Researchers Develop More Powerful and Long-lasting Battery*, J. B. Goodenough interview by J. Schroeder, https://www.tun.com/blog/university-of-texas-powerful-and-longlasting-battery/

[8] M. Sakai, *Journal of the Electrochemical Society* **167** (2020) 160540. https://dx.doi.org/10.1149/1945-7111/abcf53

[9] R. W. Gurney, *Physical Review Journals Archive* **47** (1935) 479. https://dx.doi.org/10.1103/PhysRev.47.479

[10] R. Gomer and L. W. Swanson, *The Journal of Chemical Physics* **38** (1963) 1613-1629. https://dx.doi.org/10.1063/1.1776932

[11] J. Bernard, *Adsorption on Metal Surface, Studies in Surface Science and Catalysis,* Elsevier Sci. B.V., Amsterdam, The Netherlands, 1993, p. 150. ISBN-10: 0444421637

[12] N. Sato, *Electrochemistry at Metal and Semiconductor Electrodes,* Elsevier Sci. B.V., Amsterdam, The Netherlands, 2003, p. 121-126. ISBN 0-444-82806-0

[13] T. Uehara, N. Igarashi, R. V. Belosludov, A. A. Farajian, H. Mizuseki, Y. Kawazoe, *Journal of the Japan Institute of Metals and Materials* **70(6)** (2006) 478-482. https://dx.doi.org/10.2320/jinstmet.70.478 (in Japanese)

[14] J. B. Li, K. Koumoto, H. Yanagida, *Journal of the Ceramic Society of Japan* **96(1109)** (1988) 74. https://doi.org/10.2109/jcersj.96.74

[15] T. Nakayama, K. Shiraishi, S. Miyazaki, Y. Akasaka, T. Nakaoka, K. Torii, A. Ohta, P. Ahmet, K. Ohmori, N. Umezawa, H. Watanabe, T. Chikyow, Y. Nara, H. Iwai, K. Yamada, *ECS Transactions* **3(3)** (2006) 129. https://doi.org/10.1149/1.2355705

[16] K. Shiraishi, Y. Akasaka, S. Miyazaki, T. Nakayama, T. Nakaoka, G. Nakamura, K. Torii, H. Furutou, A. Ohta, P. Ahmet, K. Ohmori, H. Watanabe, T. Chikyow, M. L. Green, Y. Nara, K. Yamada, *Technical Digest of IEEE International Electron Devices Meeting*, Washington D.C., USA, 2005, p.43-46. ISBN 9780780392687

[17] T. Nakayama, K. Shiraishi, *Hyomen Kagaku* **28(1)** (2007) 28-33. https://dx.doi.org/10.1380/jsssj.28.28 (in Japanese)

[18] K. Shiraishi, T. Nakayama, *Hyomen Kagaku* **29(2)** (2008) 92-98. https://dx.doi.org/10.1380/jsssj.29.92 (in Japanese)

[19] T. Nakayama, Y. Kangawa, and K. Shiraishi, *Atomic Structures and Electronic Properties of Semiconductor Interfaces* in *Comprehensive Semiconductor Science and Technology,* P. Bhattacharya, R. Fornari, H. Kamimura, Eds, Elsevier Sci. B. V., Amsterdam, The Netherlands, 2011, p. 157-161. ISBN 978-0-444-53153-7

[20] N. Sato, *Electrochemistry at Metal and Semiconductor Electrodes,* Elsevier Sci. B.V., Amsterdam, The Netherlands, 2003, p. 35-37. ISBN 0-444-82806-0

[21] A. J. Bard, L. R. Faulkner, *Electrochemical Methods, Fundamentals and Applications,* John Wiley & Sons, Inc., 2001 p.556. ISBN 0-471-04372-9

[22] N. Sato, *Electrochemistry at Metal and Semiconductor Electrodes,* Elsevier Sci. B.V., Amsterdam, The Netherlands, 2003, p. 39-41. ISBN 0-444-82806-0
[23] N. Sato, *Electrochemistry at Metal and Semiconductor Electrodes,* Elsevier Sci. B.V., Amsterdam, The Netherlands, 2003, p.44-45. ISBN 0-444-82806-0
[24] T. Nakayama, *Physica B* **191** (1993) 16-22. https://dx.doi.org/ 10.1016/0921-4526(93)90175-6
[25] M. Cardona, N. E. Christensen, *Physical Review* B **35** (1987) 6182. https://dx.doi.org/10.1103/PhysRevB.35.6182
[26] N. Sato, *Electrochemistry at Metal and Semiconductor Electrodes*, Elsevier Sci. B.V., Amsterdam, The Netherlands, (2003) p. 254. ISBN 0-444-82806-0
[27] I. Nakajima, *Denki Kagaku* **21** (1953) 367-375. https://doi.org/10.5796/denka.21.367 (in Japanese)
[28] J. B. Goodenough, M. H. Braga, J. A. Ferreira, J. E. Oliveira, A. J. Murchison, *Self-Charging and/or Self-Cycling Electrochemical Cells,* United States, Patent Application Publication, US 2018/0287222 A1, Oct.4 (2018)
[29] W. J. Bardeen, *Physical Review B* **71**(10) (1947) 717. https://dx.doi.org/10.1103/PhysRev.71.717
[30] A. M. Cowley, S. M. Sze, *Journal of Applied Physics* **36**(10) (1965) 3212-3232. https://dx.doi.org/10.1063/1.1702952
[31] S. Hara, *Hyomen Kagaku* **21(12)** (2000) 791-799. https://dx.doi.org/10.1380/jsssj.21.791 (in Japanese)
[32] S. Hara, *Surface Science* **494** (2001) 2805-2810. https://doi.org/10.1016/S0039-6028(01)01596-5